JACS
JOURNAL OF THE AMERICAN CHEMICAL SOCIETY
Article
Cite This: J. Am. Chem. Soc. 2017, 139, 18339−18348
pubs.acs.org/JACS

A Redox Role for the [4Fe4S] Cluster of Yeast DNA Polymerase δ

Phillip L. Bartels,[†] Joseph L. Stodola,[‡] Peter M. J. Burgers,*[,‡] and Jacqueline K. Barton*[,†]

[†]Division of Chemistry and Chemical Engineering, California Institute of Technology, Pasadena, California 91125, United States
[‡]Department of Biochemistry and Molecular Biophysics, Washington University School of Medicine, St. Louis, Missouri 63110, United States

Supporting Information

ABSTRACT: A $[4Fe4S]^{2+}$ cluster in the C-terminal domain of the catalytic subunit of the eukaryotic B-family DNA polymerases is essential for the formation of active multi-subunit complexes. Here we use a combination of electrochemical and biochemical methods to assess the redox activity of the $[4Fe4S]^{2+}$ cluster in *Saccharomyces cerevisiae* polymerase (Pol) δ, the lagging strand DNA polymerase. We find that Pol δ bound to DNA is indeed redox-active at physiological potentials, generating a DNA-mediated signal electrochemically with a midpoint potential of 113 ± 5 mV versus NHE. Moreover, biochemical assays following electrochemical oxidation of Pol δ reveal a significant slowing of DNA synthesis that can be fully reversed by reduction of the oxidized form. A similar result is apparent with photooxidation using a DNA-tethered anthraquinone. These results demonstrate that the [4Fe4S] cluster in Pol δ can act as a redox switch for activity, and we propose that this switch can provide a rapid and reversible way to respond to replication stress.

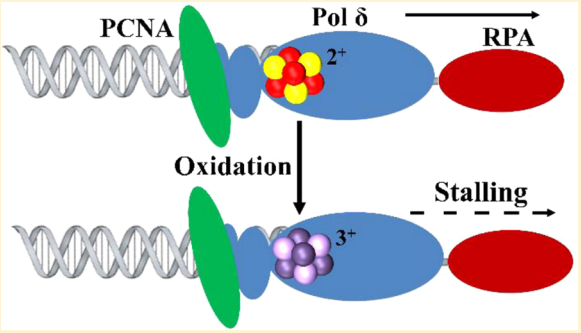

INTRODUCTION

During genomic replication, eukaryotic cells divide the task of DNA synthesis between three B-family DNA polymerases (Pols): Pol α, Pol δ, and Pol ε.[1] Each of these enzymes forms a multi-subunit complex composed of a catalytic subunit and a B-subunit, with additional accessory subunits present in Pol δ and Pol ε.[2] Recent work has shown that a $[4Fe4S]^{2+}$ cluster in the C-terminal domain (CTD) of the catalytic subunit is essential for the formation of multi-subunit complexes in the case of Pol δ.[3] Functionally, the B-family polymerases are believed to carry out DNA synthesis in a division of labor model, with the DNA primase−Pol α complex initiating 5′−3′ DNA synthesis by forming an RNA−DNA hybrid primer that is then extended by Pol ε on the continuously generated leading strand and by Pol δ on the discontinuously formed lagging strand.[4] Additional roles for Pol δ during leading strand replication have been suggested.[5,6] Pol δ is also involved in various DNA recombinatorial and repair processes.[7]

While the C-terminal [4Fe4S] cluster clearly plays a role in complex formation,[3] several lines of evidence suggest a more direct functional role. First, a 2.5 Å X-ray crystal structure of the yeast Pol α CTD in complex with its B-subunit contained zinc in place of a cluster, demonstrating that structural integrity can be supported by simpler metals.[8] Given the metabolic expense of [4Fe4S] cluster biosynthesis and loading into target proteins, the strict conservation of this cofactor in the B-family polymerases suggests that it serves an important function.[9] Indeed, the importance of [4Fe4S] clusters in these enzymes is emphasized by the presence of an additional cluster in the unique Pol ε N-terminal domain.[10]

The [4Fe4S] clusters perform a wide range of roles in biology including enzymatic catalysis and electron transfer.[11] In the DNA polymerases, the cluster is not required for catalysis.[3,12] Many DNA-processing enzymes have now been shown to contain [4Fe4S] clusters, and, in many cases, a DNA-bound redox activity of the cluster has been demonstrated.[13−16] These diverse proteins include base excision repair glycosylases, repair helicases, and DNA primase. As in the Pol δ holoenzyme, the clusters are largely redox-inert in the absence of DNA.[17−20] However, when bound to DNA, these protein cofactors undergo a significant negative shift in redox potential, activating the clusters toward oxidation.[21−23] Electrochemical experiments with DNA-bound proteins show a reversible redox signal with potentials ranging from 65 to 95 mV versus the normal hydrogen electrode (NHE).[13−16] EPR studies support the assignment of the reversible signal to the $[4Fe4S]^{3+/2+}$ couple favored by high-potential iron proteins (HiPIP) that are electron carriers.[13,24,25] In addition to modulating redox potential, the π-stacked base pairs of DNA can act as a medium for long-range charge transport between redox-active proteins.[26] DNA-mediated charge transport (DNA CT) is characterized by a shallow distance dependence and high sensitivity to base pair stacking, making it an excellent reporter of DNA integrity.[26] Importantly, although DNA CT can be attenuated by proteins that bend the duplex or flip out bases, DNA CT can proceed unimpeded through nucleosome-wrapped DNA.[26]

Received: September 26, 2017
Published: November 22, 2017

DOI: 10.1021/jacs.7b10284
J. Am. Chem. Soc. 2017, 139, 18339−18348

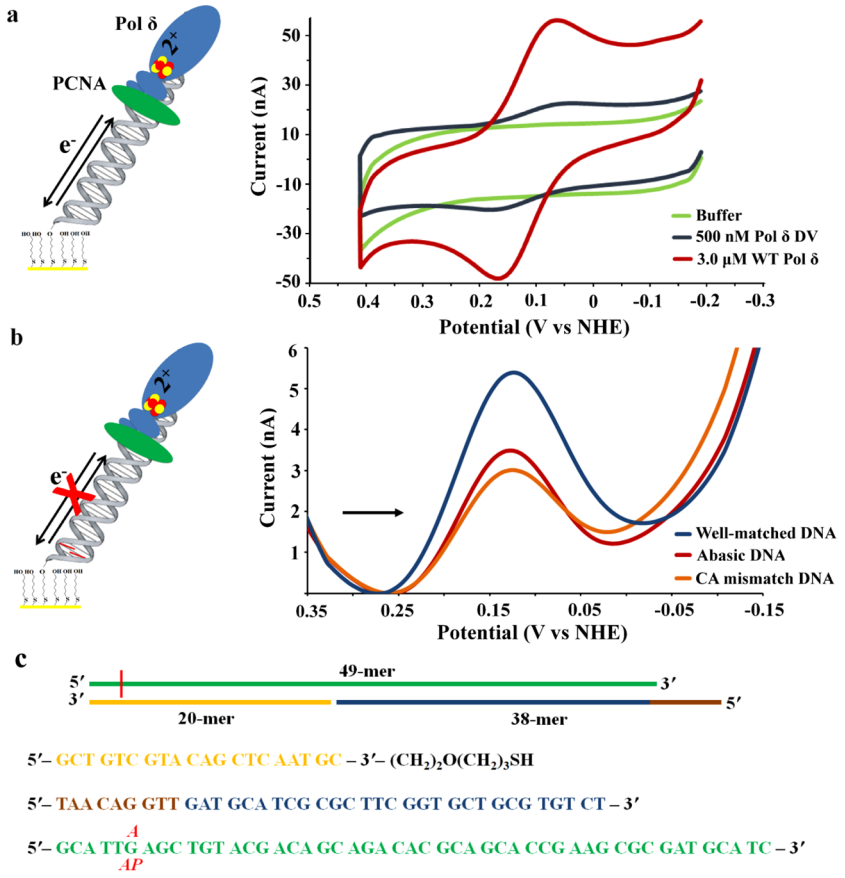

Figure 1. Electrochemical characterization of Pol δ. (a) The addition of 3.0 μM WT Pol δ and 10 μM PCNA to a DNA-modified gold electrode results in a reversible CV signal with a midpoint potential centered at 116 ± 3 mV versus NHE (red). The exonuclease-deficient mutant Pol δ DV cannot degrade DNA in the presence of catalytic magnesium, and, by including $MgAc_2$ and with 5 μM PCNA and excess dATP, signals at the same potential as WT can be obtained at concentrations as low as 500 nM (blue). (b) When an abasic site or CA mismatch is incorporated into the DNA substrate 6 nucleotides from the tethered end, signals from 500 nM Pol δ DV are attenuated by ~40% by SQWV relative to those on well-matched DNA, confirming that Pol δ is capable of DNA-mediated signaling. (c) DNA substrate design for electrochemical experiments. The substrate consists of three parts: a 20-mer thiol, a 38-mer, and a 49-mer complement. Notably, the nick in the phosphate backbone is not expected to interfere with CT. The red dash corresponds to the location of the abasic (AP) site or CA mismatch. Electrochemistry was performed in storage buffer (30 mM HEPES, pH 7.4, 350 mM NaAc, 1 mM DTT, 0.1 mM EDTA, 10% glycerol v/v, 0.01% decaethylene glycol monododecyl ether v/v), and the abasic site/mismatch discrimination experiments also included 5.0 μM PCNA, 80 μM dATP, and 8.0 mM $MgAc_2$. The CV scan rate was 100 mV/s. SQWV scans were taken at 15 Hz frequency and 25 mV amplitude, and the arrow indicates the direction of the scan.

The redox activity of the [4Fe4S] cluster appears to be utilized in many of these proteins as a switch to regulate DNA binding and therefore activity. For the DNA repair enzyme endonuclease III (EndoIII), the negative shift in redox potential associated with DNA binding has been shown to lead to a 500-fold increase in DNA binding affinity for the oxidized $[4Fe4S]^{3+}$ cluster versus the reduced 2+ form.[27] In the case of human DNA primase, the oxidation state of the [4Fe4S] cluster also controls template binding, and redox switching through electron transfer between clusters in primase and Pol α has been proposed to regulate RNA primer handoff.[16]

Here we focus on Pol δ, a central B-family polymerase. We utilize a combination of electrochemical, spectroscopic, and biochemical techniques to investigate redox activity in this enzyme and to understand the consequences of redox switching for polymerase activity. These studies provide a new perspective on polymerase regulation under oxidative stress.

MATERIALS AND METHODS

Protein Expression and Purification. Yeast Pol δ (WT and exo$^-$ D520V), replication factor C (RFC), replication protein A (RPA), proliferating cell nuclear antigen (PCNA), and *E. coli* EndoIII were expressed according to previously published protocols.[3,28]

DNA Preparation. The DNA substrate for electrochemistry consisted of a 49:58-mer primer-template composed of three oligomers: a 20-mer with a 3′-thiol modification, a 38-mer, and a 49-mer complement; sequences are as follows (see also Figure 1c):

20-mer thiol: 5′-GCT GTC GTA CAG CTC AAT GC-3′-$(CH_2)_2O(CH_2)_3SH$

38-mer: 5′-TAA CAG GTT GAT GCA TCG CGC TTC GGT GCT GCG TGT CT-3′

49-mer: 5′-GCA TT**G** AGC TGT ACG ACA GCA GAC ACG CAG CAC CGA AGC GCG ATG CAT C-3′

The bold G of the 49-mer was changed to an A or an abasic (AP) site for CA mismatch and abasic site discrimination experiments.

DNA replication assays used single-stranded M13mp18 plasmid purchased from New England Biolabs (NEB). Primers were purchased from IDT and purified by HPLC as described above. Primed DNA was formed by heating a 1:1 plasmid/primer mix in activity buffer (50 mM Tris-HCl, pH 7.8, 50 mM NaCl) to 90 °C for 5′ and cooling to RT over several hours. The M13mp18 DNA primer had the following sequence (complementary to positions 6265−6235): 5′-GAC TCT AGA GGA TCC CCG GGT ACC GAG CTC G -3′

Primers were radiolabeled by incubating 10 pmol of 31-mer M13mp18 primer with T4 polynucleotide kinase (PNK) and [γ-^{32}P]

DOI: 10.1021/jacs.7b10284
J. Am. Chem. Soc. 2017, 139, 18339−18348

ATP (PerkinElmer) in T4 buffer (NEB) for 15 min at 37 °C. Reactions were stopped by addition of EDTA to 10 mM and heating at 75 °C for 10 min. Two log DNA ladder (NEB) was dephosphorylated by calf intestinal alkaline phosphatase (CIAP; 60 min, 37 °C) prior to labeling in the same manner. As an additional size standard, duplexed M13mp18 DNA was linearized by digestion with HincII (60 min, 37 °C) and dephosphorylated by CIAP prior to radiolabeling. Proteins and unincorporated ATP were removed using spin columns (BioRad Microspin6) equilibrated in Pol δ activity buffer (50 mM Tris-HCl, pH 7.8, 50 mM NaCl). T4 PNK, CIAP, HincII, and dsM13mp18 DNA were purchased from NEB.

Pol δ Electrochemistry. All electrochemical experiments were performed using a potentiostat equipped with a multiplexer, both from CH Instruments. Experiments used a standard three-electrode cell composed of a Au working electrode, a Ag/AgCl reference electrode in 3 M NaCl (BASInc.), and a 1 mm diameter Pt wire counter electrode (Lesker). Potentials were converted from Ag/AgCl to NHE by adding 212 mV to the potential as measured by Ag/AgCl; this correction accounted for both ambient temperature and the use of 3 M NaCl for reference storage.[29] Experiments with Pol δ were all run in polymerase storage buffer (30 mM HEPES, pH 7.4, 350 mM NaAc, 1 mM DTT, 0.1 mM EDTA, 10% glycerol v/v, and 0.01% w/v decaethylene glycol monododecyl ether).

Because PCNA can slide directly onto DNA with open ends, the clamp loader complex RFC was excluded from these experiments.[30] Wild-type (WT) Pol δ 3′−5′ exonuclease activity was prevented by excluding Mg^{2+} from the buffer. In initial experiments, 3−5 μM WT Pol δ or exonuclease-deficient Pol δ D520V (DV)[31] was incubated on the electrode for several hours in the presence of 5−10 μM PCNA. To spare enzyme, later experiments used Pol δ DV at 500 nM in combination with 5.0 μM PCNA, 80 μM dATP, and 8 mM $MgAc_2$. Cyclic voltammetry (CV; 100 mV/s scan rate) and square wave voltammetry (SQWV; 15 Hz frequency, 25 mV amplitude) scans were taken once per hour for several hours. Between scans, electrodes were covered in Parafilm and stored in a humid environment to minimize evaporation. CV scan rate dependence was assessed after 3 h using rates of 20, 50, 80, 100, 200, 500, 750, and 1000 mV/s. In experiments with abasic and CA mismatch DNA, signal attenuation was calculated as follows:

$$[1 - ((\text{peak area on abasic or CA mismatch DNA})/(\text{peak area on unmodified DNA}))] \times 100\% \quad (1)$$

Pol δ concentrations are reported as the concentration of the [4Fe4S] cluster, determined by UV−visible absorbance at 400 nm (ε_{400} = 13 000 M^{-1} cm^{-1}).[3] The [4Fe4S] cluster loading was in the range of 70−85%, determined by dividing [4Fe4S] concentration by total protein concentration as measured by Bradford assay, Pierce BCA assay, and UV−visible absorbance at 280 nm (ε_{280} = 194 100 M^{-1} cm^{-1}; estimated using the EXPasy ProtParam tool). Bradford and BCA assay standard curves were generated using a BSA standard, and both kits were purchased from Thermo Scientific. UV−visible spectra were taken on a Cary Varian instrument using 100 μL quartz cuvettes purchased from STARNA Cells.

When possible, diffusion coefficients were obtained from the scan rate dependence of the CV current using the Randles−Sevcik equation:[32]

$$I_p = [0.4463(F^3/RT)^{1/2}](n^{3/2})(A)(D^{1/2})(C^\circ)\nu^{1/2} \quad (2)$$

I_p is the peak current in amperes, F is Faraday's constant (96485 C·mol^{-1}), R is the universal gas constant (8.314 J·$(mol·K)^{-1}$), T is temperature in K, n is the number of electrons transferred per CV peak, A is electrode area in cm^2, D is the diffusion coefficient in $cm^2·s^{-1}$, C° is bulk protein concentration in mol·cm^{-3}, and ν is the scan rate in V·s^{-1}. Experimental values of D were compared to those estimated by the Stokes−Einstein equation,

$$D = k_B T/6\pi\eta R \quad (3)$$

where k_B is Boltzmann's constant (1.38 × 10^{-23} J·K^{-1}), T is the incubation temperature (293 K), η is the solution viscosity (estimated to be 1.38 × 10^{-3} Pa·s for an aqueous solution with 10% glycerol), and R is the hydrodynamic radius. R was estimated to be ∼26 Å from dimensions obtained from X-ray crystal structures of DNA-bound Pol3, Pol1-Pol12, and PCNA (PDB ID 3IAY, 3FLO, and 4YHR, respectively).

Electrochemical Oxidation and Spectroscopic Analysis of Pol δ. To prevent cluster degradation in the presence of O_2, bulk electrolysis was performed in an anaerobic glovebag (COY) under a 95% N_2, 5% H_2 atmosphere with an O_2-scavenging catalyst present. Buffers were degassed by bubbling in argon for several hours and stored open in the glovebag overnight prior to experiments. For spectroscopic characterization, a 150 μL sample of 1−2 μM Pol δ was added to two identical DNA-modified electrodes. On one electrode, a potential of 0.412 V vs NHE was applied for ∼15 min, while no potential was applied to the other. Oxidation yields were estimated by taking the difference between the total charge obtained in the presence of Pol δ and that generated by electrolysis with buffer alone. Following electrolysis, UV−visible and electron paramagnetic resonance (EPR) spectroscopy were used to confirm the integrity of the cluster after electrolysis. Samples were sealed in cuvettes for UV−visible spectroscopy and subsequently returned to the glovebag and added to EPR tubes. Tubes were sealed by Parafilm and frozen in liquid nitrogen outside the bag. Continuous-wave X-band EPR was performed at 10 K, and each experiment consisted of nine sweeps taken at 12.88 mW microwave power, 2 G modulation amplitude, and 5.02 × 10^3 receiver gain.

Pol δ Activity Assays. Immediately prior to assays, Pol δ DV was oxidized on Au rod electrodes exactly as described for spectroscopic characterization, but the sample was diluted to 190 nM in degassed storage buffer in a total volume of 30−40 μL. Reduction of oxidized sample was carried out at a potential of −0.188 V vs NHE for a similar length of time. In parallel with electrolysis, 140 μL reaction mixes (0.1 mg/mL BSA, 80 μM each deoxynucleotide triphosphate (dNTP), 500 μM ATP, 2.0 nM M13mp18 with a ^{32}P-labeled primer, 8.0 mM $MgAc_2$, 500 nM RPA, 5.0 nM RFC, 5.0 nM PCNA, 50 mM NaCl, 50 mM Tris-HCl, pH 7.8) were prepared inside the glovebag. The PCNA sliding clamp was loaded onto the primer end by incubating the reaction mix with the RFC clamp loader and ATP for 1 min at 30 °C. After clamp loading, reactions were initiated by the addition of 2 nM (final concentration) oxidized, untreated, or rereduced Pol δ DV. Reactions were run at 30 °C, and 20 μL aliquots were removed and quenched at specific time points by adding 10 μL of stop mix (10 mM EDTA and 0.1% v/v SDS final concentration). The polymerase was heat-inactivated for 10−20 min (55 °C), and samples were counted on a liquid scintillation counter to determine exposure time (1 h per 300 000 counts). Samples were dried on a speed vacuum and dissolved in alkaline gel buffer (500 mM NaOH, 10 mM EDTA) with 1× alkaline loading dye (6× stock: 300 mM NaOH, 6.0 mM EDTA, 18% Ficoll w/v, 0.25% xylene cyanol w/v, and 0.15% bromocresol green w/v), and equivalent amounts of radioactivity were then loaded onto a 1% alkaline agarose gel and run at 30 V for 14−15 h. Gels were neutralized in 7% trichloroacetic acid (w/v) in water for 30 min at RT, dried under mild pressure for several hours, exposed on a phosphor screen, and visualized on a Typhoon phosphorimager (GE Healthcare). Products were analyzed using ImageQuant software (GE Healthcare). The relative amounts of DNA synthesis were determined by dividing the volume of the largest band in an oxidized sample by the equivalent band in the appropriate untreated sample.

To limit DNA synthesis to that of a single processive cycle by the PCNA−Pol δ complex, 0.01 mg/mL heparin was included in reactions[33] that were then analyzed on 5% polyacrylamide gels. In these instances, Pol δ was added after clamp loading and reactions were started by adding a mix of dNTPs and heparin. Quenched reactions were then counted, dried, and redissolved in 2.0 μL of formamide loading dye. Immediately prior to gel loading, samples were heated at 90 °C for 10 min, and gels were run at ∼50 W for 5 h in 1× Tris-borate-EDTA buffer. Polyacrylamide gels were then exposed and imaged by phosphorimager analysis.

DOI: 10.1021/jacs.7b10284
J. Am. Chem. Soc. 2017, 139, 18339−18348

Tris-HCl, NaCl, $MgAc_2$, BSA, and heparin were purchased from Sigma-Aldrich, while dNTPs and ATP were from NEB. dNTPs, ATP, and $MgAc_2$ were thoroughly degassed prior to reaction, and the protein stocks were kept open during a series of vacuum/nitrogen/gas mix purges to minimize residual oxygen.

Chemical Oxidation of Pol δ. For photooxidation, the 31-mer M13mp18 primer was covalently modified with a 5′-anthraquinone (AQ). AQ was prepared as a phosphoramidite and added to the unmodified DNA on a DNA synthesizer according to previously reported procedures.[34] The presence of AQ was verified by MALDI-TOF, and the modified primer was annealed to M13mp18 DNA in Pol δ activity buffer (50 mM Tris-HCl, pH 7.8, 50 mM NaCl). Because the 5′-AQ modification prevented ^{32}P end-labeling, DNA was labeled by adding 2 μCi [α-^{32}P] dATP (PerkinElmer) to the reaction, and incorporation of [α-^{32}P] dATP was facilitated by lowering the concentration of cold dATP from 80 μM to 10 μM.

Anaerobic reaction mixes lacking dNTPs were prepared in glass vials and incubated under a solar simulator equipped with a UVB/C long-pass filter or in the dark for 30 min. To ensure complete oxidation, 2-fold molar excesses of both PCNA and Pol δ DV were included. As controls, reactions were also run using unmodified DNA (no AQ), and AQ reactions were repeated with 140 nM Klenow fragment exo$^-$ (NEB). After treatment, samples were returned to the glovebag and transferred into Eppendorf tubes containing dNTPs to start the reaction. Free dNTPs were removed using BioRad Microspin 6 columns in SCC buffer (GE Healthcare), and sample radioactivity was quantified on a liquid scintillation counter. Samples were then run out on a 1% alkaline agarose gel and visualized by phosphorimaging analysis. Overall [α-^{32}P] dATP incorporation was used to compare overall DNA synthesis levels by dividing the total radioactivity counts in oxidized samples by those of dark controls.

RESULTS

Electrochemical Characterization of Pol δ. To determine whether Pol δ holoenzyme was redox active in the presence of DNA, we carried out electrochemistry on DNA-modified gold electrodes. In initial experiments, 3 μM WT Pol δ in storage buffer was combined with 10 μM PCNA and incubated on the electrode for several hours. CV scans taken hourly reveal a reversible signal with a midpoint potential of 116 ± 3 mV vs NHE (Figure 1a). This signal grows in over time to reach a maximum size of 41 ± 4 nC and −51 ± 2 nC for the reductive and oxidative peaks at a 100 mV/s scan rate after 2 h of incubation (Figure 1). The CV current varies linearly with the square root of the scan rate (Figure S1), as expected of a diffusive rather than adsorbed species.[32] The diffusive nature of the signal is in agreement with earlier studies of DNA-binding proteins.[14] No differences were observed between aerobic and anaerobic electrochemistry carried out in a glovebag, indicating that the cluster is relatively stable in air and consistent with the general long-term stability of B-family DNA polymerases.[35] The redox couple observed was attributed to the $[4Fe4S]^{3+/2+}$ based on the fact that Pol δ is HiPIP-like, being EPR-silent unless oxidized.[3] In addition, the electrochemical signal is similar to the DNA glycosylases EndoIII and MutY, in which the identity of the couple has been established by EPR.[13,24]

We could obtain quantifiable signals at lower concentrations by adding dNTPs and Mg^{2+} to enhance protein association with the DNA. To prevent degradation of the DNA substrate by the 3′−5′ exonuclease activity of WT Pol δ, we turned to the exonuclease-deficient mutant Pol δ DV (D520V) for these experiments.[31] At 113 ± 5 mV vs NHE, the midpoint potential of Pol δ DV is indistinguishable from WT (Figure 1, S3). By adding 80 μM dATP (the incoming nucleotide), 8.0 mM $MgAc_2$, and 5.0 μM PCNA, we were able to see signals with Pol δ concentrations as low as 500 nM (Figure 1). Under these conditions, the maximum CV peak areas were 6.9 ± 1 nC and −7.5 ± 1 nC for the reductive and oxidative peaks at a scan rate of 100 mV/s.

The midpoint potential of Pol δ is within the HiPIP potential regime, but it is slightly higher than the 65−95 mV vs NHE reported for DNA-bound repair proteins.[13,28] We used the well-studied *E. coli* BER glycosylase EndoIII[28] to determine if the measured potential is truly distinct or the result of different buffer conditions. In our standard phosphate buffer (20 mM sodium phosphate, pH 7.5, 100 mM NaCl, 1 mM EDTA, 10% glycerol v/v), the EndoIII midpoint potential is ∼80 mV versus NHE.[28] However, when we exchanged EndoIII into Pol δ storage buffer, CV and SQWV carried out with 140 or 1.5 μM EndoIII result in a midpoint potential of 113 ± 3 mV versus NHE, which is indistinguishable from Pol δ (Figure S2b). UV−visible spectra confirm the stability of EndoIII in Pol δ buffer (Figure S2a). The observed increase in EndoIII potential is most likely due to the significantly higher ionic strength of Pol δ storage buffer (350 mM NaAc in Pol δ buffer vs 150 mM NaCl in EndoIII buffer).[36,37] In any case, the fact that the EndoIII and Pol δ redox potentials are indistinguishable under identical buffer conditions supports the assertion that the [4Fe4S] cluster resides in the same narrow potential regime in both proteins.

Given that Pol δ ordinarily functions in complex with PCNA, we next asked what effect PCNA might have on the electrochemical properties of Pol δ. In the absence of PCNA, the midpoint potential is unaltered at 115 ± 8 mV versus NHE, but the signal was markedly smaller, reaching a maximum CV peak area of 0.4 ± 0.1 nC for the reductive peak and −0.7 ± 0.1 nC for the oxidative peak (Figure S3). The signal also decays more rapidly with PCNA absent, suggesting lower polymerase stability in the absence of PCNA. To compare the signals with and without PCNA more quantitatively, diffusion coefficients (D) under both conditions were calculated using the Randles−Sevcik equation.[32] At maximum signal size, D was found to be $(6.7 \pm 3) \times 10^{-6}$ $cm^2 \cdot s^{-1}$ with PCNA and dATP present, which is within 1 order of magnitude of an estimate (6.0×10^{-7} $cm^2 \cdot s^{-1}$) based on the Stokes−Einstein equation. The difference between these values most likely reflects errors from the use of multiple partial crystal structures to estimate the hydrodynamic radius. In the absence of PCNA, D decreases to $(1.2 \pm 0.3) \times 10^{-7}$ $cm^2 \cdot s^{-1}$, which is on the same order of magnitude as the value estimated from the Stokes−Einstein equation. These results are consistent with differently shaped complexes, in agreement with the known elongated form of Pol δ alone in solution and the more compact form expected when multiple subunits have engaged with PCNA.[3,38] To see if dNTPs contribute to the shape of PCNA-bound Pol δ, we prepared a surface with Pol δ and PCNA but lacking dATP and Mg^{2+}. Under these conditions, the signal is comparable to that in the absence of PCNA, giving a D value of $(2.2 \pm 0.7) \times 10^{-7}$ $cm^2 \cdot s^{-1}$. Taken together, these results indicate that PCNA does not affect the potential of Pol δ but is critical for effective DNA binding, and the entire complex is more likely to remain DNA-bound when dNTPs are present.

To determine if the Pol δ signal is DNA-mediated, we carried out electrochemistry using DNA containing either an abasic site or a CA mismatch 6 nucleotides from the thiolated end (Figure 1c). In addition to base stack integrity, DNA-mediated signaling in proteins is dependent on film morphology, with DNA-bound proteins capable of charge transport both through the DNA

DOI: 10.1021/jacs.7b10284
J. Am. Chem. Soc. 2017, 139, 18339−18348

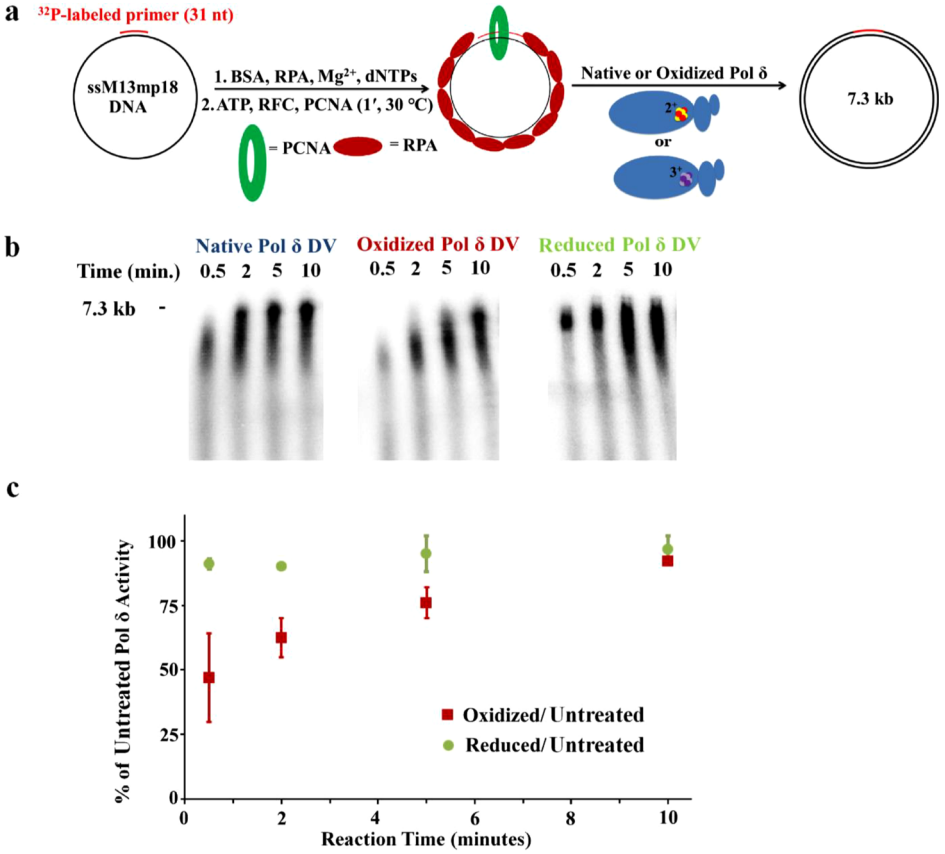

Figure 2. Activity assays with native and electrochemically oxidized Pol δ DV. (a) 190 nM Pol δ DV was oxidized or reduced by bulk electrolysis at potentials of 0.412 and −0.188 V and subsequently diluted to 2 nM final concentration into reaction mixes containing radiolabeled M13mp18 DNA. (b, c) As seen on representative 1% alkaline agarose gels, oxidation lowers activity levels at early time points, while reduction restores activity to native levels. The degree of this effect can be quantified by dividing the amount of DNA synthesis in reactions with oxidized or reduced Pol δ by that from reactions with untreated enzyme. The oxidation yield for the gel shown in b is ∼80%. Error bars are standard deviation of the mean ($n \geq 3$).

bases and directly through the monolayer surface (Figure S4).[28] In general, closely packed monolayers provide more DNA that may be less accessible to large proteins, while the opposite is true of loosely packed monolayers. To address all of these issues together, we prepared monolayers in the presence of 100 mM $MgCl_2$ to form closely packed islands of DNA (30−50 pmol·cm^{-2}) in parallel with standard loosely packed monolayers (15−20 pmol·cm^{-2}) formed without Mg^{2+} (Figure S4).[39,40] For both morphologies, half of each chip contained well-matched DNA, and the other half contained either abasic or CA mismatch DNA (Figure S4a). In all experiments, we used 500 nM Pol δ DV in the presence of PCNA, dATP, and $MgAc_2$.

Consistent with previous studies on EndoIII,[28] Pol δ redox potentials are identical on both film morphologies, supporting the assertion that all observed signals are from DNA-bound proteins (Figure S4). On closely packed DNA films, signal size is highly variable, but 46 ± 33% signal attenuation as determined by SQWV was observed on abasic DNA (Figure S4). No mismatch discrimination was observed, and even the abasic site discrimination decreased over time as more protein diffused to the surface. In general, the signals on closely packed monolayers are consistent with variable DNA accessibility and significant steric hindrance causing protein−DNA complexes to lie flat on the surface (Figure S4). In contrast, loosely packed monolayers show very consistent signal sizes and significant charge attenuation on both DNAs containing abasic sites and CA mismatches, reaching a maximum of 44 ± 16% on abasic DNA and 46 ± 29% on CA-mismatch DNA after 2 h of incubation as measured by SQWV (Figure 1, Figure S4). Abasic site and mismatch discrimination also remain stable over time, indicating that DNA accessibility and steric hindrance are not significant problems on loosely packed DNA. Together, these results confirm that Pol δ is capable of DNA-mediated signaling and emphasize the importance of substrate accessibility when assessing CT by large protein complexes.

Activity Assays with Oxidized and Reduced Pol δ. Having seen that DNA binding can activate Pol δ for redox activity, we next asked how the cluster oxidation state might affect polymerase activity. As purified, Pol δ exists largely in the $[4Fe4S]^{2+}$ state,[3] so any assessment of activity differences would require extensive oxidation to generate sufficient amounts of the $[4Fe4S]^{3+}$ cluster for comparison. To this end, we turned to bulk electrolysis on DNA-modified electrodes, applying an oxidizing potential of 0.412 V versus NHE for 15−20 min. To prevent aerobic degradation of the oxidized cluster, all experiments were performed in a glovebag under a 95% N_2/5% H_2 atmosphere.

To achieve high yields, bulk electrolysis is best done on an electrode with a relatively large surface area. Multiplexed chips have many advantages for electrochemical characterization, but only a single electrode can be addressed at a time, and each sample in a quadrant is distributed between four electrodes. To overcome these limitations, we switched to single gold rod

DOI: 10.1021/jacs.7b10284
J. Am. Chem. Soc. 2017, 139, 18339−18348

electrodes for these experiments. In order to characterize this system, a sample of concentrated (150 μL of 2.74 μM) Pol δ was oxidized on a DNA-modified electrode in a custom-made glass cell for several hours (Figure S5a,b). UV−visible spectra were taken before and after electrolysis, after which the sample was then frozen for EPR in parallel with untreated protein (Figure S5c,d). The [4Fe4S] cluster oxidation generally results in a broad increase in UV−visible absorbance from 300 to 450 nm with a less distinct peak at 410 nm in both the $[4Fe4S]^{3+}$ and $[3Fe4S]^{+}$ species.[41−43] After bulk electrolysis, increased absorbance from 300 to 400 nm, consistent with cluster oxidation, was indeed observed. No significant increase in absorbance at 800 nm occurred after oxidation, and the 280 nm peak associated with aromatic and thiolated amino acid residues remained distinct. From our own observations, protein aggregation tends to generate a U-shaped curve with high absorbance at 800 nm and a shallow, poorly defined peak at 280 nm, and the lack of these features in our spectra indicates that oxidized Pol δ did not aggregate (Figure S5c). EPR signals are small as a result of the low sample concentration, but clear signals at g = 2.08 and g = 2.02 are present in the oxidized sample (Figure S5d). These signals are consistent with a combination of $[4Fe4S]^{3+}$ and $[3Fe4S]^{+}$ cluster oxidation products.[24,42,43] A smaller signal at g = 2.02 was also present in the native sample, consistent with earlier reports of residual $[3Fe4S]^{+}$ cluster in untreated Pol δ.[3] That some $[3Fe4S]^{+}$ cluster would occur upon oxidation is not surprising, and similar results have been obtained for EndoIII and MutY.[13,24] In earlier studies, loss of iron was attributed in part to damage incurred upon freezing, which may have also happened here. Furthermore, oxidized Pol δ was stored away from protective DNA long enough to take a UV−visible spectrum prior to freezing. In any case, some $[4Fe4S]^{3+}$ cluster was still observed, and the $[3Fe4S]^{+}$ cluster that did occur would have formed as a degradation product of the $[4Fe4S]^{3+}$ cluster.[13]

Because activity assays require only low nanomolar polymerase concentrations, bulk electrolysis for these experiments was carried out with 190 nm Pol δ DV to minimize sample waste. Oxidation yields under these conditions were higher, typically around 75−90% as determined from the total charge passed. After electrolysis, untreated or oxidized Pol δ DV was added directly to premade reaction mixes to a final concentration of 2 nM (Figure 2a). When run out on an alkaline agarose gel, it is apparent that at early time points less DNA synthesis was carried out by oxidized Pol δ (Figure 2b, S6a). DNA synthesis can be more quantitatively compared for the oxidized versus untreated sample by dividing the amount of frontier products (highest molecular weight major products) in the oxidized sample by the amount present in untreated samples. Using this analysis, oxidized Pol δ at 60−80% yield forms only 30−50% as many large (∼5 kb) DNA products as untreated Pol δ after 30 s (Figure 2c). Significantly, higher oxidation yields lead to lower activity levels. In any case, this difference gradually decreases over the course of 10 min. Regardless of oxidation state, no DNA synthesis occurs in samples lacking PCNA, confirming that all observed DNA synthesis is processive (Figure S6c).

Reduction of the oxidized Pol δ stock by electrolysis at −0.188 V versus NHE effectively restores DNA synthesis, reaching 90% of untreated levels at early time points (Figure 2b,c, Figure S6b). Critically, this result both confirms the reversibility of oxidative slowing and provides support for the $[4Fe4S]^{3+}$ cluster as the major oxidation product. As mentioned earlier, the reversible electrochemical signals are consistent with $[4Fe4S]^{3+/2+}$ cycling, but EPR spectroscopy with oxidized Pol δ showed evidence of both $[4Fe4S]^{3+}$ and $[3Fe4S]^{+}$ products in the sample, leading to some ambiguity. However, the nearly complete restoration of native activity levels upon rereduction would not be expected if most of the cluster had degraded to the $[3Fe4S]^{+}$ state, supporting the $[4Fe4S]^{3+}$ cluster as the major oxidation product. These combined results thus indicate that the $[3Fe4S]^{+}$ cluster seen by EPR likely forms after the $[4Fe4S]^{3+}$ major product degrades over time in the absence of DNA; we have observed this previously with sample freezing for *E. coli* EndoIII and MutY following chemical oxidation.[13,24]

To gain further insight into the effect of oxidation, reaction rates were estimated by comparing frontier velocities. Velocities were calculated by dividing the amount of the largest quantifiable band of DNA by time and the number of polymerase molecules present.[44] This method yields maximum rates of 118 ± 63 (SD, n = 7) nt/s per enzyme for untreated Pol δ and 21 ± 27 (SD, n = 5) nt/s for oxidized Pol δ at 2 min. The rates obtained for untreated Pol δ are consistent with previously published *in vitro* results,[33] while the oxidized form is significantly slower. This calculation represents just an upper estimate, as typical bulk electrolysis fails to oxidize around 20−30% of the enzyme; thus, some of the DNA synthesis observed in oxidized samples can be attributed to the nonoxidized population. Indeed, the comparable amounts of DNA synthesis observed after 5−10 min could have resulted from either slow oxidized polymerase catching up or redistribution of residual native Pol δ in the oxidized sample. Overall, it is clear from these experiments that oxidation leads to a decrease in replication rate, but resolution on alkaline agarose gels is insufficient to distinguish between complete stalling or dramatic slowing of DNA synthesis.

To distinguish between stalling and slowing of DNA synthesis by oxidized Pol δ, reactions were analyzed on 5% polyacrylamide gels to obtain increased resolution in the 30−1000 nucleotides range. In addition, DNA synthesis was limited to that of a single processive cycle by the PCNA−Pol δ complex by adding heparin, which traps dissociated Pol δ.[33] Without the heparin trap, products up to 7 kb were observed, due to multiple processive cycles of synthesis (Figure 2, Figure S6). In order to visualize products at all sizes, reactions containing heparin were divided in two, with half loaded onto a polyacrylamide gel and half onto an alkaline agarose gel. With heparin present, alkaline agarose gels demonstrate a severe limitation to DNA synthesis, with no products larger than ∼1 kb observed on alkaline agarose gels (data not shown). When these products are resolved on polyacrylamide gels, a greater proportion of both very small (∼primer length) and very large (∼1 kb) products are formed by untreated Pol δ, while the oxidized form generates more intermediate products between 30 and 1000 nucleotides (Figure S7).

These results illustrate several important points about the effects of oxidation on Pol δ DNA synthesis. First, they verify that the oxidized form remains active and does not completely stall. Second, the relatively greater amounts of very small products and unextended primers in reactions with native sample indicate greater susceptibility to dissociation from DNA and trapping by heparin, while the native form that does associate produces longer products. In contrast, oxidized Pol δ leaves fewer primers unextended or fully extended, instead making more intermediate products between 150 bp and 1 kb. The greater proportion of extended primers is consistent with tighter DNA binding after cluster oxidation, as has been

DOI: 10.1021/jacs.7b10284
J. Am. Chem. Soc. 2017, 139, 18339−18348

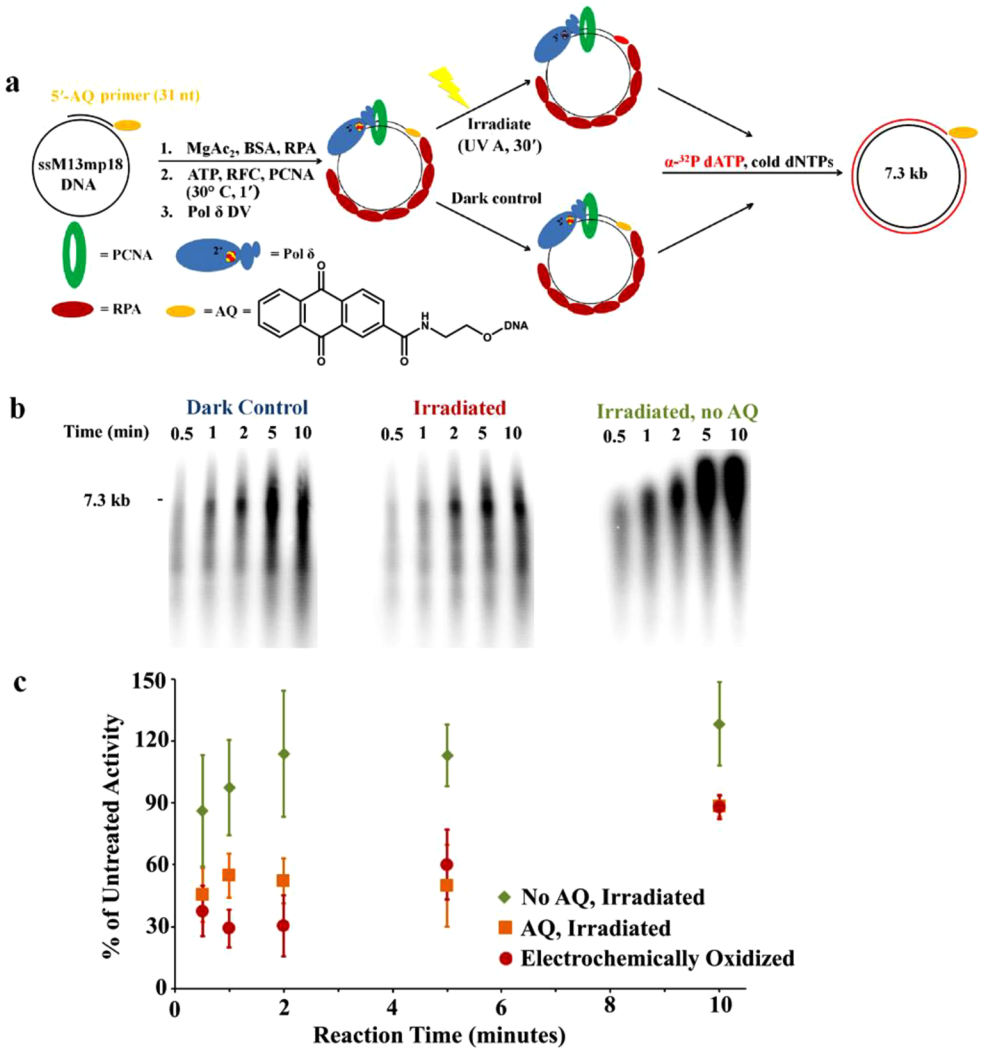

Figure 3. Pol δ activity assays with an AQ photooxidant. (a) Pol δ DV was added to a reaction mix lacking dNTPs and either irradiated under a solar simulator (UVA) or left in the dark, after which dNTPs (including [α-^{32}P] dATP) were added to start the reaction. (b, c) 1% alkaline agarose gels show less DNA synthesis by irradiated Pol δ at early time points, matching the pattern of electrochemical oxidation. Irradiation in the absence of AQ resulted in no significant effects, indicating that AQ was oxidizing the cluster. This pattern is apparent in relative radioactivity counts (or gel quantification for electrochemical oxidation), which further emphasizes the similarity between oxidation methods. Error bars are standard deviation of the mean ($n \geq 3$).

observed with both primase and DNA repair proteins.[16,27] However, the slower procession indicates that tighter binding impedes rapid procession, acting as a brake on PCNA-mediated DNA synthesis. These experiments suggest that the similar activity levels observed on alkaline agarose gels at time points beyond 5 min could be explained by either the oxidized form gradually catching up or redistribution of the residual native enzyme in the sample. Regardless of the precise details, the overall impact of polymerase stalling, with a 6-fold decrease in rate, would be significant on the time scale of S-phase; unperturbed yeast S-phase lasts ~30 min, while using oxidized Pol δ moving at 20 nt/s to replicate the lagging strand of the yeast genome would itself require 27 min.[45−47]

Chemical Oxidation of Pol δ with Anthraquinone. Electrochemical oxidation provides clear advantages in estimating yields and rereducing the oxidized sample, but the use of chemical oxidants is much more common. Thus, we were interested to see if chemical oxidation could yield an equivalent result. To this end, we used an anthraquinone-derived photooxidant covalently tethered to the 5′ end of the DNA primer.[34,48] AQ has the advantage of oxidizing samples in a DNA-mediated fashion instead of the less effective, direct oxidation of the protein by oxidants in solution.[3,48] Irradiation at 350 nm of AQ generates an excited triplet state capable of oxidizing DNA bases, and AQ has been studied extensively in the context of DNA CT.[48−50] The DNA base of lowest potential, guanine, has a redox potential of 1.29 V, which is considerably higher than that of the Pol δ [4Fe4S] cluster at 113 mV.[51] The presence of AQ on the primer, however, prevents 5′ ^{32}P end-labeling, so [α-^{32}P] dATP added to reactions was used as an alternative label (Figure 3a). Since [α-^{32}P] dATP is not necessarily incorporated in a 1:1 ratio with DNA-primed ends, activity levels were compared by total scintillation counts rather than by directly quantifying gel bands.

Following irradiation, samples with AQ showed lower overall DNA synthesis relative to identical samples kept in the dark (Figure 3b,c). As with electrochemistry, the maximum differentials occur at earlier time points. After 30 and 60 s, irradiated Pol δ showed 40−60% of dark control DNA

DOI: 10.1021/jacs.7b10284
J. Am. Chem. Soc. 2017, 139, 18339−18348

synthesis. In contrast, reaction mixes irradiated in the presence of unmodified DNA are not significantly different from dark controls at early time points and remain equal or greater throughout the time course (Figure 3c, Figure S8). Similarly, no significant differences are observed between reactions with irradiated or untreated *E. coli* Klenow fragment exo$^-$ on AQ-modified DNA (Figure S8), indicating that the attenuation observed in Pol δ DNA synthesis can be attributed to [4Fe4S] cluster oxidation. Assuming the activity differential at early time points approximated the percentage of oxidized sample, as was the case electrochemically, photooxidation yields ranged from 40% to 50%. Overall, the pattern of attenuated activity after photooxidation is consistent with the results from electrochemical experiments (Figure 3c), independently confirming the slowing of Pol δ upon cluster oxidation.

DISCUSSION

In this work, we have demonstrated that the [4Fe4S] cluster of DNA polymerase δ can serve an important functional role as a redox-active cofactor that regulates enzymatic activity. On DNA-modified gold electrodes, Pol δ shows a reversible signal with a midpoint potential of 113 ± 5 mV versus NHE. Notably, this potential is comparable to that of the previously characterized [4Fe4S] protein EndoIII under the same buffer conditions. Charge attenuation in the presence of either an abasic site or a CA mismatch confirms that the redox signal is DNA-mediated. Activity assays carried out with electrochemically oxidized Pol δ demonstrate that oxidation results in significant slowing of processive DNA synthesis; the same result occurs following irradiation in the presence of an anthraquinone photooxidant. An assessment of both large and small DNA products indicates that the oxidized form remains active, but it is less processive. Given the retention of activity with decreased processivity, these results are consistent with an increase in DNA binding affinity upon oxidation, which would impede rapid sliding of PCNA-bound Pol δ. A significant increase in DNA binding is evident also with EndoIII upon oxidation.[27] Critically, reduction by bulk electrolysis largely restores activity to native levels, confirming that cluster oxidation acts as a reversible switch. The reversibility of oxidation also lends further support to our electrochemical and spectroscopic evidence for the $[4Fe4S]^{3+}$ cluster as the biologically relevant oxidation product rather than the degraded $[3Fe4S]^{+}$ cluster. Taken as a whole, these results suggest that reversible oxidation of the [4Fe4S] cluster in Pol δ could provide a rapid and reversible way to respond to replication stress.

Replication stress is a general term for fork slowing or stalling due to factors such as dNTP depletion, UV irradiation, and oxidative stress.[52] Both replicative helicases and polymerases are known to be stabilized at stalled forks independently of checkpoint kinase activity, although the mechanism of stabilization and its relationship to global checkpoint regulation remains incompletely understood.[53] Pol δ slowing through cluster oxidation would be a straightforward way to stall replication on the lagging strand, and this form of slowing could also complement more standard regulatory mechanisms. In general, Pol δ slowing would lead to accumulation of single-stranded DNA and RPA on the lagging strand, activating checkpoint kinases that could then stall the helicase by phosphorylation of key subunits.[54,55] Among other types of stress, oxidative stress and ionizing radiation carry a heightened risk of double-strand break formation.[56] Furthermore, reactive oxygen species generate lesions such as 8-oxoguanine (OxoG), which is highly mutagenic due to the propensity of replicative polymerases to generate OxoG:A mispairs.[57] Oxidation of the [4Fe4S] cluster from the 2+ to 3+ form could occur either directly, by reactive oxygen species, or, more likely, by charge transport communication through double-stranded DNA with other oxidized species. Previously, we have seen that guanine radicals, the precursors to OxoG, can carry out DNA CT to oxidize the [4Fe4S] cluster of DNA-bound EndoIII.[24] An additional benefit of polymerase stalling by DNA-mediated oxidation would be the prevention of excessive DNA synthesis under high risk circumstances. In addition to preventing damage, redox signaling to and from Pol δ could play a role in fork reversal and recombination events associated with replication stress.[52,58]

A general model for redox regulation of Pol δ is shown in Figure 4. In this model, processive lagging strand replication proceeds until replication stress occurs and the Pol δ $[4Fe4S]^{2+}$ cluster is oxidized either directly or by an electron acceptor, possibly an oxidized [4Fe4S] protein or a guanine radical formed during oxidative stress. We have found, in the case of EndoIII, that cluster oxidation promotes a substantial increase in binding affinity.[27] Here, given the already tight binding to DNA of Pol δ with PCNA, a still tighter binding causes Pol δ to slow its progression. The slowing of lagging strand synthesis would lead to RPA accumulation and an activation of checkpoint signaling, ultimately resulting in repair or replication fork collapse. Once the conditions of stress resolve, lagging strand synthesis can be restored by reduction of the Pol δ $[4Fe4S]^{3+}$ cluster, likely by another [4Fe4S] protein involved in DNA processing. Importantly, only Pol δ bound to the DNA in a complex with PCNA is readily oxidized, leaving the bulk of unbound Pol δ in the reduced 2+ form. Furthermore, this

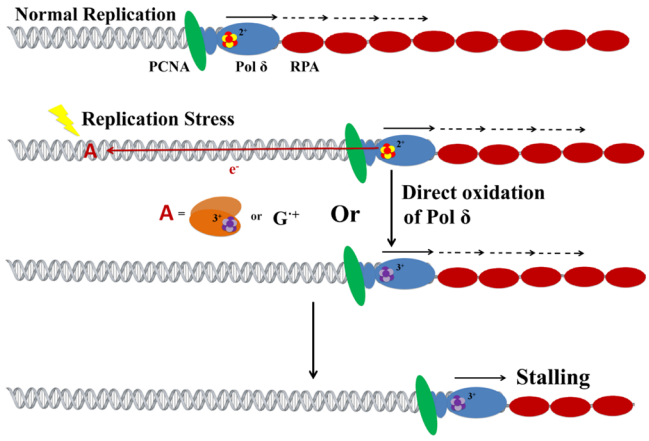

Figure 4. Model for redox-mediated regulation of Pol δ activity. Under ordinary circumstances, Pol δ forms a complex with PCNA and processively extends lagging strand DNA (top). When replication stress occurs, lagging strand synthesis could be stalled either by transfer of an electron from the Pol δ $[4Fe4S]^{2+}$ cluster to an acceptor (A) or by direct oxidation of the DNA-bound Pol δ–PCNA complex. In the case of DNA-mediated oxidation, the electron acceptor could be an oxidized [4Fe4S] protein or a guanine radical cation, $\mathbf{G}^{\bullet+}$, formed during oxidative stress. Once the cluster is oxidized to the $[4Fe4S]^{3+}$ form, Pol δ binds more tightly to DNA and synthesis slows. After damage resolution, lagging strand replication could be restored by reduction of the $[4Fe4S]^{3+}$ cluster by another [4Fe4S] protein.

DOI: 10.1021/jacs.7b10284
J. Am. Chem. Soc. 2017, 139, 18339–18348

signaling can occur rapidly and at distance through DNA-mediated CT.

It is interesting to consider the many possible partners for DNA CT with Pol δ in the context of this model. First, Pol δ could be directly oxidized by species formed during oxidative stress, such as the guanine radical cation.[24] After removal of reactive oxygen species, a partner [4Fe4S] protein could then rereduce Pol δ and restore lagging strand replication. Alternatively, the entire redox cycle could be carried out between Pol δ and other [4Fe4S] proteins associated with the replication fork. The nuclease−helicase Dna2 is a prime example of such a partner, as it associates with the replication fork and is involved in both fork reversal and double-strand break repair.[59,60] In human cells, the [4Fe4S] DNA repair glycosylase MUTYH associates with PCNA during S-phase; whether this association also occurs in the yeast homologue, Ntg2, is not known.[61] If the glycosylases do generally associate with the fork, redox signaling could enable rapid communication between replication and repair pathways in eukaryotes. Finally, redox signaling between Pol δ and the B-family translesion DNA synthesis polymerase Pol ζ could help these proteins to hand off DNA-containing bulky lesions. Indeed, a role for the cluster in the Pol δ−Pol ζ switch has already been suggested.[62] In this view, Pol δ and Pol ζ switch by exchanging their shared B-subunits, although this would leave the cluster vulnerable to degradation.[63] However, a redox handoff similar to that suggested between primase and Pol α could allow such a transfer without requiring direct subunit exchange.[16] While redox control of Pol δ would provide clear opportunities and is intriguing to consider, the *in vivo* mechanism and possible partners still require further investigation.

In summary, we have shown that Pol δ can use its [4Fe4S] cluster for reversible electron transfer along DNA and that oxidation of the cluster leads to reversible stalling. Taken together, our data suggest a model in which Pol δ uses redox signaling through DNA to sense oxidative stress, stalling replication under the mutagenic conditions, and potentially coordinating activities with repair and other replication proteins. Overall, the redox sensitivity of Pol δ reveals the oxidation state of the [4Fe4S] cluster to be a critical redox switch to rapidly and reversibly respond to replication stress.

■ ASSOCIATED CONTENT

Supporting Information

The Supporting Information is available free of charge on the ACS Publications website at DOI: 10.1021/jacs.7b10284.

DNA synthesis and purification for electrochemistry, preparation of DNA-modified gold electrodes, DNA substrate design, scan rate dependence, UV−visible spectra and CV of EndoIII in polymerase buffer, Pol δ SQWV ± PCNA, bulk electrolysis and spectroscopic characterization, full alkaline agarose gels, polyacrylamide gel analysis, AQ assay with *E. coli* Klenow fragment (PDF)

■ AUTHOR INFORMATION

Corresponding Authors

*burgers@wustl.edu
*jkbarton@caltech.edu

ORCID

Jacqueline K. Barton: 0000-0001-9883-1600

Notes

The authors declare no competing financial interest.

■ ACKNOWLEDGMENTS

We are grateful to the NIH (GM120087 to J.K.B., GM118129 to P.M.B.) and US-Israel Binational Science Foundation (2013358 to P.M.B.) for their financial support of this work.

■ REFERENCES

(1) Lujan, S. A.; Williams, J. S.; Kunkel, T. A. *Trends Cell Biol.* **2016**, *26*, 640−654.
(2) Johansson, E.; MacNeill, S. A. *Trends Biochem. Sci.* **2010**, *35*, 339−347.
(3) Netz, D. J. A.; Stith, C. M.; Stümpfig, M.; Köpf, G.; Vogel, D.; Genau, H. M.; Stodola, J. L.; Lill, R.; Burgers, P. M. J.; Pierik, A. J. *Nat. Chem. Biol.* **2012**, *8*, 125−132.
(4) Burgers, P. M. J.; Kunkel, T. A. *Annu. Rev. Biochem.* **2017**, *86*, 417−438.
(5) Johnson, R. E.; Klassen, R.; Prakash, L.; Prakash, S. *Mol. Cell* **2015**, *59*, 163−175.
(6) Yeeles, J. T. P.; Janska, A.; Early, A.; Diffley, J. F. X. *Mol. Cell* **2017**, *65*, 105−116.
(7) Prindle, M. J.; Loeb, L. A. *Environ. Mol. Mutagen.* **2012**, *53*, 666−682.
(8) Klinge, S.; Núñez-Ramírez, R.; Llorca, O.; Pellegrini, L. *EMBO J.* **2009**, *28*, 1978−1987.
(9) Netz, D. J. A.; Mascarenhas, J.; Stehling, O.; Pierik, A. J.; Lill, R. *Trends Cell Biol.* **2014**, *24*, 303−312.
(10) Jain, R.; Vanamee, E. S.; Dzikovski, B. G.; Buku, A.; Johnson, R. E.; Prakash, L.; Prakash, S.; Aggarwal, A. K. *J. Mol. Biol.* **2014**, *426*, 301−308.
(11) Johnson, D. C.; Dean, D. R.; Smith, A. D.; Johnson, M. K. *Annu. Rev. Biochem.* **2005**, *74*, 247−281.
(12) Swan, M. K.; Johnson, R. E.; Prakash, L.; Prakash, S.; Aggarwal, A. K. *Nat. Struct. Mol. Biol.* **2009**, *16*, 979−986.
(13) Boal, A. K.; Yavin, E.; Lukianova, O. A.; O'Shea, V. L.; David, S. S.; Barton, J. K. *Biochemistry* **2005**, *44*, 8397−8407.
(14) Mui, T. P.; Fuss, J. O.; Ishida, J. P.; Tainer, J. A.; Barton, J. K. *J. Am. Chem. Soc.* **2011**, *133*, 16378−16381.
(15) Grodick, M. A.; Segal, H. M.; Zwang, T. J.; Barton, J. K. *J. Am. Chem. Soc.* **2014**, *136*, 6470−6478.
(16) O'Brien, E.; Holt, M. E.; Thompson, M. K.; Salay, L. E.; Ehlinger, A. C.; Chazin, W. J.; Barton, J. K. *Science* **2017**, *355*, 813.
(17) Porello, S. L.; Cannon, M. J.; David, S. S. *Biochemistry* **1998**, *37*, 6465−6475.
(18) Fan, L.; Fuss, J. O.; Cheng, Q. J.; Arvai, A. S.; Hammel, M.; Roberts, V. A.; Cooper, P. K.; Tainer, J. A. *Cell* **2008**, *133*, 789−800.
(19) Ren, B.; Duan, X.; Ding, H. *J. Biol. Chem.* **2009**, *284*, 4829−4835.
(20) Weiner, B. E.; Huang, H.; Dattilo, B. M.; Nilges, M. J.; Fanning, E.; Chazin, W. J. *J. Biol. Chem.* **2007**, *282*, 33444−33451.
(21) Gorodetsky, A. A.; Boal, A. K.; Barton, J. K. *J. Am. Chem. Soc.* **2006**, *128*, 12082−12083.
(22) Bartels, P. L.; Zhou, A.; Arnold, A. R.; Nuñez, N. N.; Crespilho, F. N.; David, S. S.; Barton, J. K. *Langmuir* **2017**, *33*, 2523−2530.
(23) Ha, Y.; Arnold, A. R.; Nuñez, N. N.; Bartels, P. L.; Zhou, A.; David, S. S.; Barton, J. K.; Hedman, B.; Hodgson, K. O.; Solomon, E. I. *J. Am. Chem. Soc.* **2017**, *139*, 11434−11442.
(24) Yavin, E.; Boal, A. K.; Stemp, E. D. A.; Boon, E. M.; Livingston, A. L.; O'Shea, V. L.; David, S. S.; Barton, J. K. *Proc. Natl. Acad. Sci. U. S. A.* **2005**, *102*, 3546−3551.
(25) Dey, A.; Jenney, F. E.; Adams, M. W. W.; Babini, E.; Takahashi, Y.; Fukuyama, K.; Hodgson, K. O.; Hedman, B.; Solomon, E. I. *Science* **2007**, *318*, 1464−1468.
(26) Arnold, A. R.; Grodick, M. A.; Barton, J. K. *Cell Chem. Biol.* **2016**, *23*, 183−197.
(27) Tse, E. C. M.; Zwang, T. J.; Barton, J. K. *J. Am. Chem. Soc.* **2017**, *139*, 12784−12792.

DOI: 10.1021/jacs.7b10284
J. Am. Chem. Soc. 2017, 139, 18339−18348

(28) Pheeney, C. G.; Arnold, A. R.; Grodick, M. A.; Barton, J. K. *J. Am. Chem. Soc.* **2013**, *135*, 11869−11878.
(29) Greeley, R. S.; Smith, W. T.; Stoughton, R. W.; Lietzke, M. H. *J. Phys. Chem.* **1960**, *64*, 652−657.
(30) Burgers, P. M. J.; Yoder, B. L. *J. Biol. Chem.* **1993**, *268*, 19923−19926.
(31) Garg, P.; Stith, C. M.; Sabouri, N.; Johansson, E.; Burgers, P. M. *Genes Dev.* **2004**, *18*, 2764−2773.
(32) Kissinger, P. T.; Heineman, W. R. *Laboratory Techniques in Electroanalytical Chemistry*, 2nd ed.; Kissinger, P. T.; Heineman, W. R., Eds.; Marcel Dekker: New York, 1996; pp 51−139.
(33) Stodola, J. L.; Burgers, P. M. *Nat. Struct. Mol. Biol.* **2016**, *23*, 402−408.
(34) Schaefer, K. N.; Barton, J. K. *Biochemistry* **2014**, *53*, 3467−3475.
(35) Johnson, R. E.; Prakash, L.; Prakash, S. *Methods Enzymol.* **2006**, *408*, 390−407.
(36) Tomoaki, O.; Nakamura, H.; Katsumi, N.; Cusanovich, M. A.; Aktus, H. *Biophys. J.* **1998**, *75*, 1483−1490.
(37) Lode, E. T.; Murray, C. L.; Rabinowitz, J. C. *J. Biol. Chem.* **1976**, *251*, 1683−1687.
(38) Johansson, E.; Majka, J.; Burgers, P. M. *J. Biol. Chem.* **2001**, *276*, 43824−43828.
(39) Boon, E. M.; Salas, J. E.; Barton, J. K. *Nat. Biotechnol.* **2002**, *20*, 282−286.
(40) Kelley, S. O.; Barton, J. K.; Jackson, N. M.; Hill, M. G. *Bioconjugate Chem.* **1997**, *8*, 31−37.
(41) Sweeney, W. V.; Rabinowitz, J. C. *Annu. Rev. Biochem.* **1980**, *49*, 139−161.
(42) Johnson, M. K.; Duderstadt, R. E.; Duin, E. C. *Adv. Inorg. Chem.* **1999**, *47*, 1−82.
(43) Duff, J. L. C.; Breton, J. L. J.; Butt, J. N.; Armstrong, F. A.; Thomson, A. J. *J. Am. Chem. Soc.* **1996**, *118*, 8593−8603.
(44) Hedglin, M.; Pandey, B.; Benkovic, S. J. *Proc. Natl. Acad. Sci. U. S. A.* **2016**, *113*, 201523653.
(45) Kulak, N. A.; Pichler, G.; Paron, I.; Nagaraj, N.; Mann, M. *Nat. Methods* **2014**, *11*, 319−324.
(46) Goffeau, A.; Barrell, B. G.; Bussey, H.; Davis, R. W.; Dujon, B.; Feldmann, H.; Galibert, F.; Hoheisel, J. D.; Jacq, C.; Johnston, M.; Louis, E. J.; Mewes, H. W.; Murakami, Y.; Philippsen, P.; Tettelin, H.; Oliver, S. G. *Science* **1996**, *274*, 546−567.
(47) Lengronne, A.; Pasero, P.; Bensimon, A.; Schwob, E. *Nucleic Acids Res.* **2001**, *29*, 1433−1422.
(48) Henderson, P. T.; Jones, D.; Hampikian, G.; Kan, Y.; Schuster, G. B. *Proc. Natl. Acad. Sci. U. S. A.* **1999**, *96*, 8353−8358.
(49) Armitage, B.; Yu, C.; Devadoss, C.; Schuster, G. B. *J. Am. Chem. Soc.* **1994**, *116*, 9847−9859.
(50) Gasper, S. M.; Schuster, G. B. *J. Am. Chem. Soc.* **1997**, *119*, 12762−12771.
(51) Nuñez, M. E.; Hall, D. B.; Barton, J. K. *Chem. Biol.* **1999**, *6*, 85−97.
(52) Berti, M.; Vindigni, A. *Nat. Struct. Mol. Biol.* **2016**, *23*, 103−109.
(53) De Piccoli, G.; Katou, Y.; Itoh, T.; Nakato, R.; Shirahige, K.; Labib, K. *Mol. Cell* **2012**, *45*, 696−704.
(54) Zeman, M. K.; Cimprich, K. A. *Nat. Cell Biol.* **2014**, *16*, 2−9.
(55) Saldivar, J. C.; Cortez, D.; Cimprich, K. A. *Nat. Rev. Mol. Cell Biol.* **2017**, *18*, 622−636.
(56) Azzam, E. I.; Jay-Gerin, J. P.; Pain, D. *Cancer Lett.* **2012**, *327*, 48−60.
(57) McCulloch, S. D.; Kokoska, R. J.; Garg, P.; Burgers, P. M.; Kunkel, T. A. *Nucleic Acids Res.* **2009**, *37*, 2830−2840.
(58) Zellweger, R.; Dalcher, D.; Mutreja, K.; Berti, M.; Schmid, J. A.; Herrador, R.; Vindigni, A.; Lopes, M. *J. Cell Biol.* **2015**, *208*, 563−579.
(59) Thangavel, S.; Berti, M.; Levikova, M.; Pinto, C.; Gomathinayagam, S.; Vujanovic, M.; Zellweger, R.; Moore, H.; Lee, E. H.; Hendrickson, E. A.; Cejka, P.; Stewart, S.; Lopes, M.; Vindigni, A. *J. Cell Biol.* **2015**, *208*, 545−562.
(60) Nimonkar, A. V.; Genschel, J.; Kinoshita, E.; Polaczek, P.; Campbell, J. L.; Wyman, C.; Mdrich, P.; Kowalczykowski, S. C. *Genes Dev.* **2011**, *25*, 350−362.
(61) Markkanen, E.; Dom, J.; Hübscher, U. *Front. Genet.* **2013**, *4*, 18.
(62) Baranovskiy, A. G.; Lada, A. G.; Siebler, H. M.; Zhang, Y.; Pavlov, Y. I.; Tahirov, T. H. *J. Biol. Chem.* **2012**, *287*, 17281−17287.
(63) Johnson, R. E.; Prakash, L.; Prakash, S. *Proc. Natl. Acad. Sci. U. S. A.* **2012**, *109*, 12455−12460.

DOI: 10.1021/jacs.7b10284
J. Am. Chem. Soc. 2017, 139, 18339−18348

A Redox Role for the [4Fe4S] Cluster of Yeast DNA Polymerase δ

Phillip L. Bartels[1], Joseph L. Stodola[2], Peter M.J. Burgers[2,*], and Jacqueline K. Barton[1,*]

Supporting Information

DNA synthesis and purification for electrochemistry. Thiol-modified DNA sequences were prepared by standard phosphoramidite chemistry on a DNA synthesizer (Applied Biosystems) using A, G, C, T phosphoramidites and the 3′-Thiol-Modifier 6-S-S CPG as purchased from Glen research. DNA substrates were cleaved and deprotected by 8-hour incubation in NH_4OH (Sigma-Aldrich) at 65 □. Deprotected DNA was separated from truncation products by reverse-phase HPLC (Agilent PLRPS column, gradient of 5 – 75% ACN/95 - 25% 50 mM NH_4Ac over 30 minutes at a 2 mL/min flow rate). Thiol-modified DNA was reduced by dissolving in 50 μL Tris, pH 8.0 (Qiagen elution buffer), adding excess DTT (Sigma-Aldrich), and shaking for 45 minutes. DTT was removed by filtration through a NAP-5 column (GE Healthcare) prior to a final round of HPLC purification (gradient of 5 – 15% ACN/95 – 85% 50 mM NH_4Ac over 35 minutes at 2 mL/min). Lastly, single-stranded DNA was desalted by standard ethanol precipitation (100 μl water, 1 mL 100% EtOH, 130 mM NaCl) and the identity of the substrate was confirmed by MALDI-TOF. Unmodified oligomers were ordered from IDT and purified by the DMT-free HPLC method. Desalted DNA was dissolved in a phosphate storage

buffer (5 mM sodium phosphate, 50 mM NaCl, pH 7.0) and concentrations were determined by UV-visible spectroscopy using ε_{260} values estimated by Integrated DNA Technologies (IDT). Equimolar concentrations of single stranded DNA were then degassed and annealed (rapid heating to 95^{o} C, 5-minute incubation, and 1.5 hour cooling to 20 ^{o} C).

Preparation of DNA-modified Gold Electrodes. Multiplexed chips containing 16 Au electrodes (0.015 cm^2 area) were prepared as described previously (*64*). Self-assembled monolayers (SAMs) were formed by incubating 25 μL of 25 μM duplexed DNA on the electrode overnight, after which electrodes were rinsed 3-5 times in phosphate buffer (5 mM sodium phosphate, pH 7.5, 50 mM NaCl) and backfilled for 45 minutes with 1 mM 6-mercapto-1-hexanol (Sigma-Aldrich) in the same buffer containing 5% (v/v) glycerol. Electrodes were then extensively rinsed in phosphate buffer followed by protein storage buffer (30 mM HEPES, pH 7.4, 350 mM NaAc, 1 mM DTT, 0.1 mM EDTA, 10% glycerol, and 0.01% decaethylene glycol monododecyl ether). Lastly, the absence of electroactive impurities was confirmed by scanning the surface with cyclic voltammetry (CV).

Bulk electrolysis experiments were undertaken by droplet electrochemistry (30-40 μL solution) on Au rod electrodes of 0.0314 cm^2 electrode area (Pine Research Instrumentation). Electrodes were cleaned as previously described (*65*), and monolayers formed using the same procedure as the multiplexed chip.

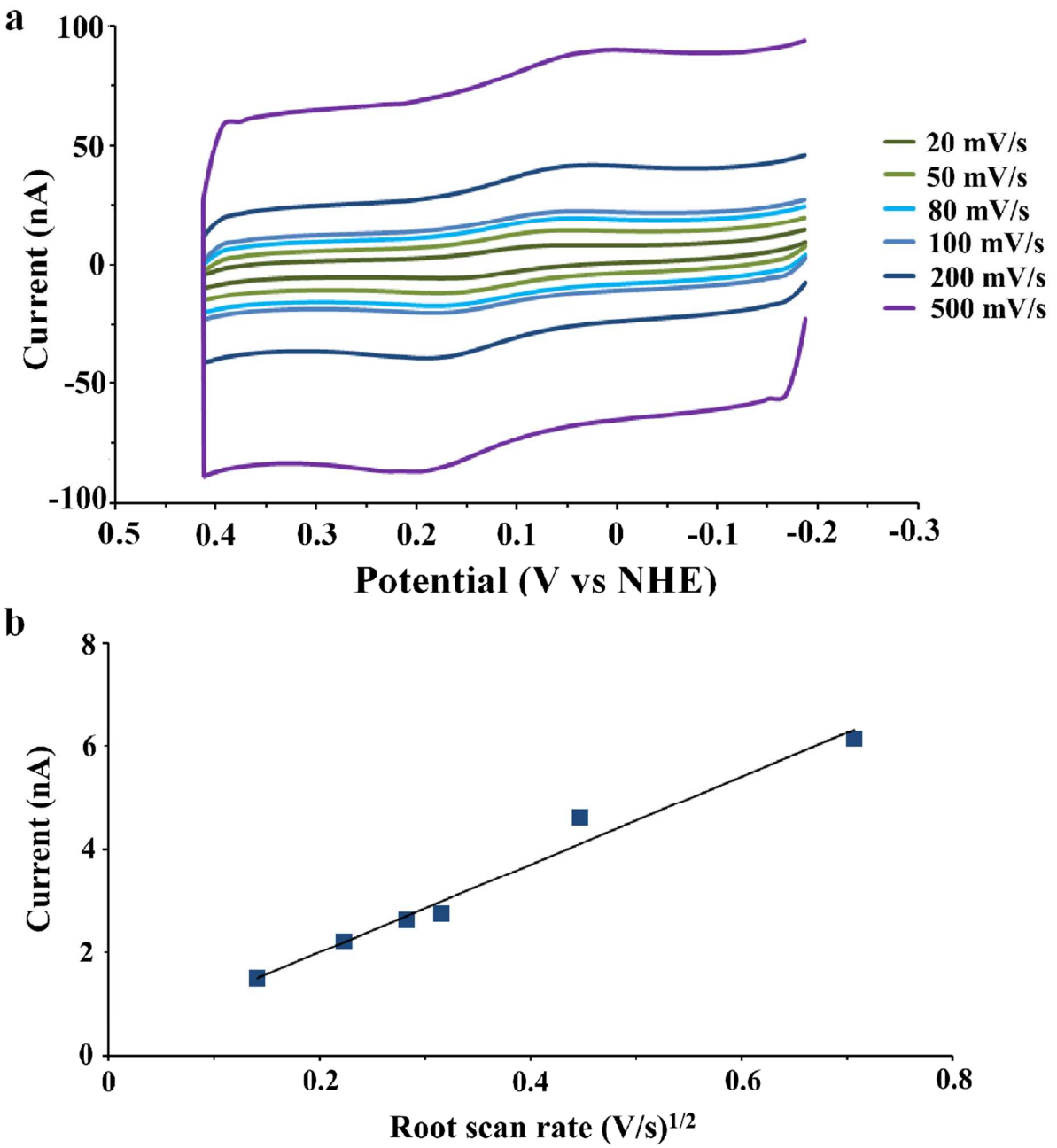

Figure S1. Scan rate dependence of the CV current in 500 nM Pol δ DV incubated with 5.0 μM PCNA, 80 μM dATP, and 8.0 mM $MgAc_2$. (**a**) The maximum peak current increases with increasing scan rate, coupled with an increase in peak splitting. (**b**) The current exhibits a linear dependence on the square root of the scan rate, characteristic of a diffusive rather than adsorbed species. The scan rates included are 20, 50, 80, 100, 200, and 500 mV/s. The line was fit to data averaged from 8 separate experiments, and the fit is $I = 7.7559\nu^{1/2} + 0.5725$ with an R^2 value of 0.9828.

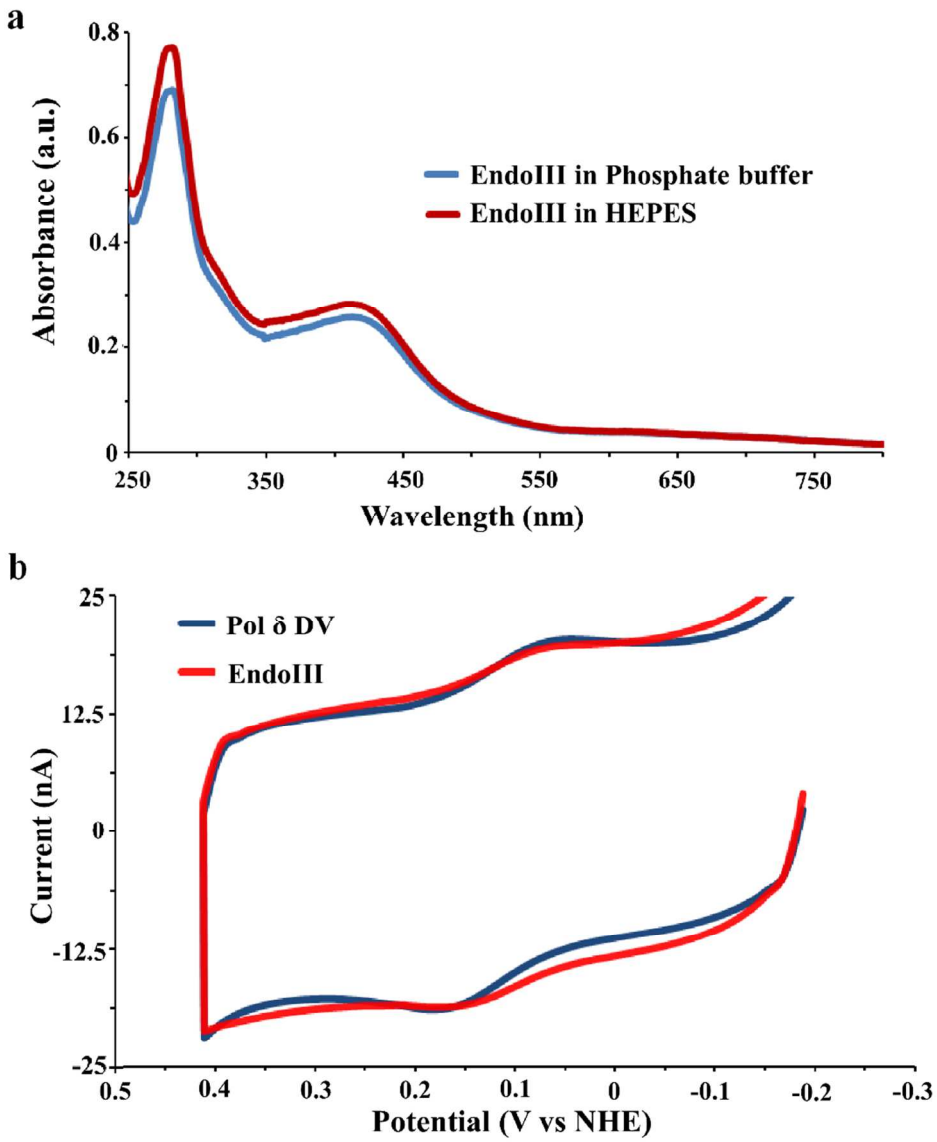

Figure S2. Pol δ and EndoIII electrochemistry compared. 1.5 μM EndoIII (stored in 20 mM sodium phosphate, pH 7.5, 150 mM NaCl, 1 mM EDTA) was exchanged into Pol δ storage buffer (30 mM HEPES, pH 7.4, 350 mM NaAc, 1 mM DTT, 0.1 mM EDTA, 10% v/v glycerol, 0.01% decaethylene glycol monododecyl ether w/v) and added to a multiplexed chip containing unmodified Pol δ DNA (49:58-mer substrate). (**a**)UV-visible spectra taken before and after buffer exchange confirm the stability of EndoIII in a HEPES-based buffer. (**b**) The midpoint potential as measured by CV is 113 ± 3 mV, virtually indistinguishable from Pol δ DV at 113 ± 5 mV versus NHE.

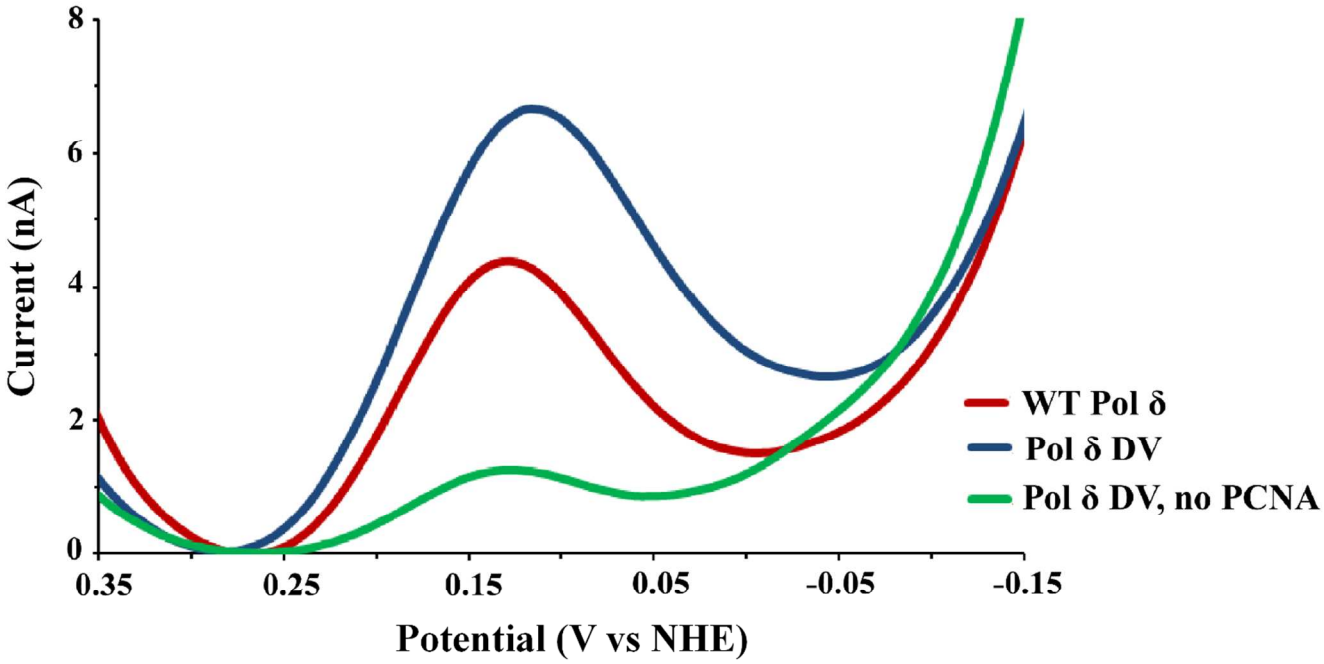

Figure S3. SQWV of 500 nM WT Pol δ and exonuclease-deficient Pol δ DV with and without 5.0 μM PCNA. WT and exo$^-$ Pol δ DV share the same potential, and both generate a substantial signal on a DNA-modified gold electrode; the smaller size of the WT signal may be due in part to DNA degradation by exonuclease activity. PCNA itself does not affect the potential, but its absence results in significantly decreased signal size and lower stability over time. SQWVs were taken at 15 Hz frequency and 25 mV amplitude, and electrochemistry was carried out in storage buffer (20 mM HEPES, pH 7.4, 350 mM NaAc, 1 mM DTT, 0.1 mM EDTA, 10% glycerol v/v, 0.01% decaethylene glycol monododecyl ether v/v) with 8.0 mM $MgAc_2$ and 80 μM dATP.

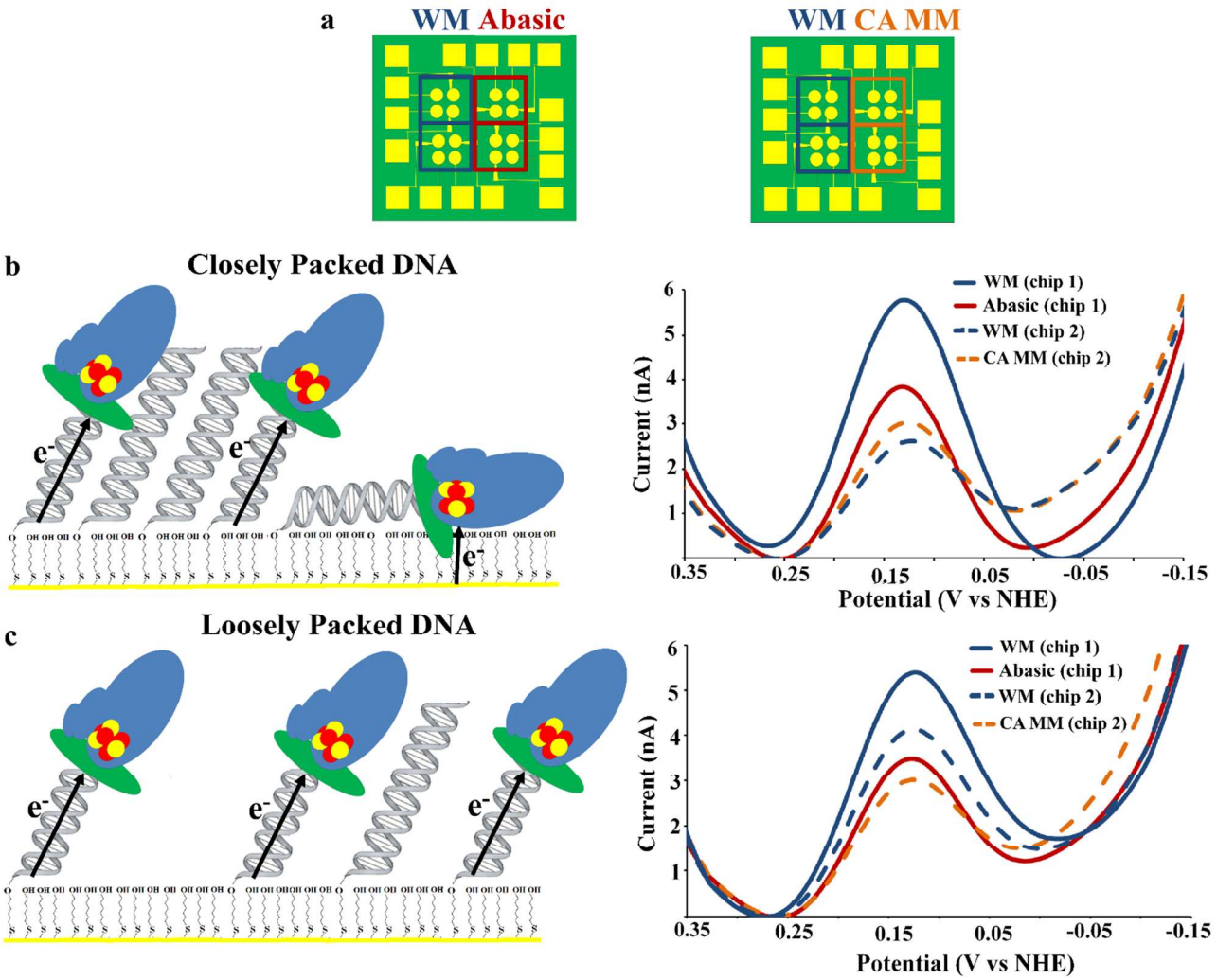

Figure S4. Pol δ electrochemistry on different DNA monolayer morphologies. (**a**) To find an optimal DNA monolayer morphology for Pol δ signaling, we prepared multiplexed chips containing either closely packed (assembled with 100 mM $MgCl_2$) or loosely packed (no $MgCl_2$) DNA films. Two chips were prepared for both morphologies, with one half of each chip consisting of well-matched (WM) DNA (dark blue) and the other containing DNA with either an abasic site (red) or a CA mismatch (orange) 6 nucleotides from the monolayer surface. (**b**) On closely packed films, Pol δ SQWV signals were highly variable and showed 46 ± 33% attenuation on abasic DNA (solid SQWV traces) but no significant mismatch discrimination (dashed SQWV traces). (**c**) In contrast, SQWV signals on loosely packed films were much more consistent between electrodes, with a 44 ± 16% signal loss on abasic DNA (solid traces) and 46 ± 29% signal loss with CA mismatch DNA (dashed traces). To minimize the effects of variability between devices, all direct comparisons were made on a single chip; scans that were directly compared are denoted by either solid or dashed lines in the SQWV signals shown. The SQWV traces shown are an average of 6 individual electrodes on a single device, with scans taken at 15 Hz frequency and 25 mV amplitude.

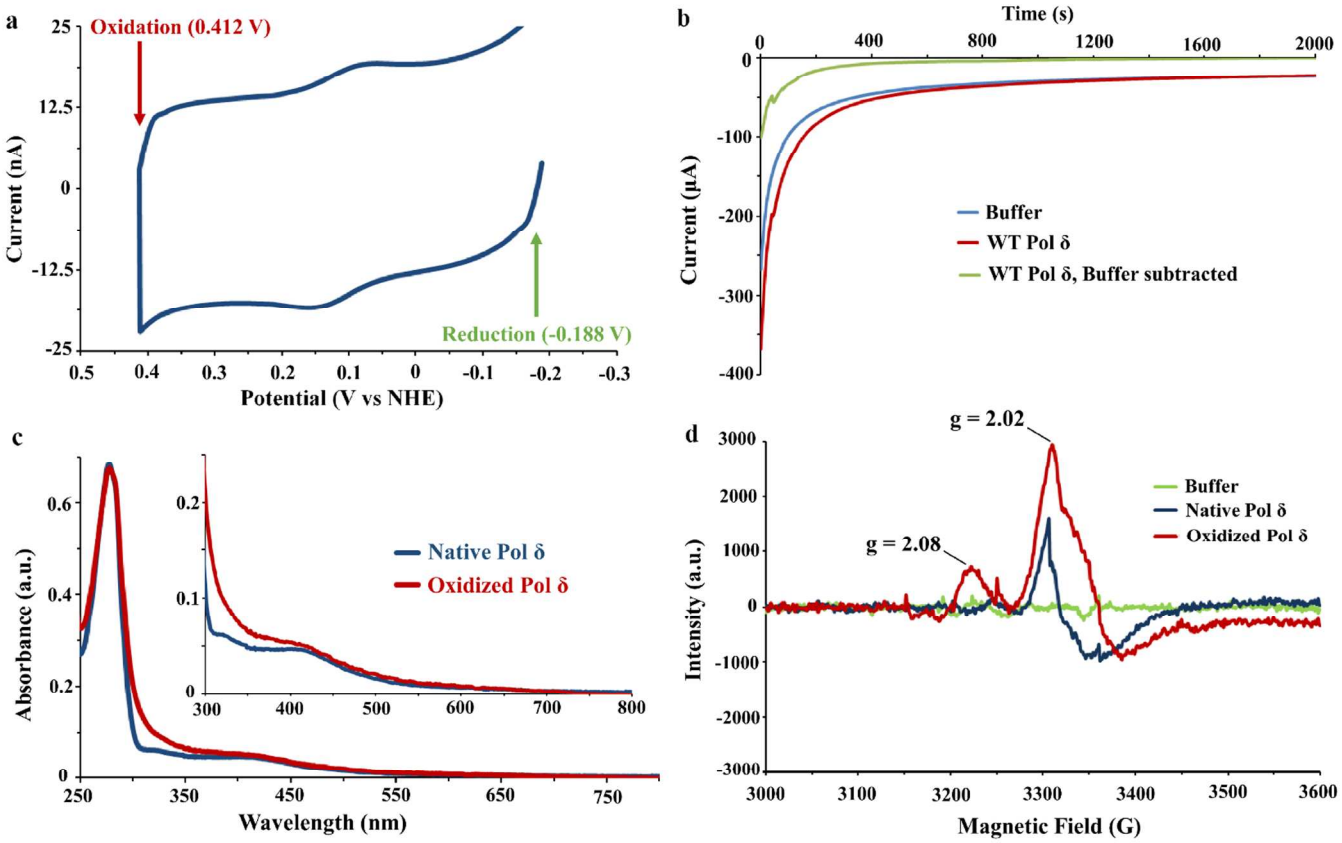

Figure S5. Characterization of electrochemically oxidized Pol δ. (**a**) Bulk electrolysis potentials were ~200 mV beyond the major oxidative and reductive peaks at 0.412 V (oxidation) and -0.188 V (reduction) versus NHE. (**b**) Yields were calculated by subtracting a background electrolysis (blue) from one containing protein (red) and taking the area under the resultant curve (green). Electrolysis of 150 µL of 2.74 µM Pol δ at 0.412 V gave ~35% oxidation yield. (**c**) UV-visible spectra reveal an increased absorbance from 300-400 nm consistent with cluster oxidation with no evidence of protein aggregation. (**d**) CW X-band EPR spectra at 10 K reveal the presence of both $[4Fe4S]^{3+}$ (g = 2.08) and $[3Fe4S]^{+}$ (g = 2.02) species in the oxidized sample, with a residual amount of $[3Fe4S]^{+}$ cluster present in the native sample. These results are consistent with the formation of $[4Fe4S]^{3+}$ cluster after anaerobic bulk electrolysis, with some degrading to form $[3Fe4S]^{+}$ cluster in the absence of DNA. As slight sample loss did occur following oxidation, the UV-visible spectrum of oxidized Pol δ has been normalized to native absorbance at 280 nm to afford a more direct comparison. EPR spectra were taken at 12.85 mW microwave power, 2 G modulation amplitude, and a receiver gain of 5.02×10^3.

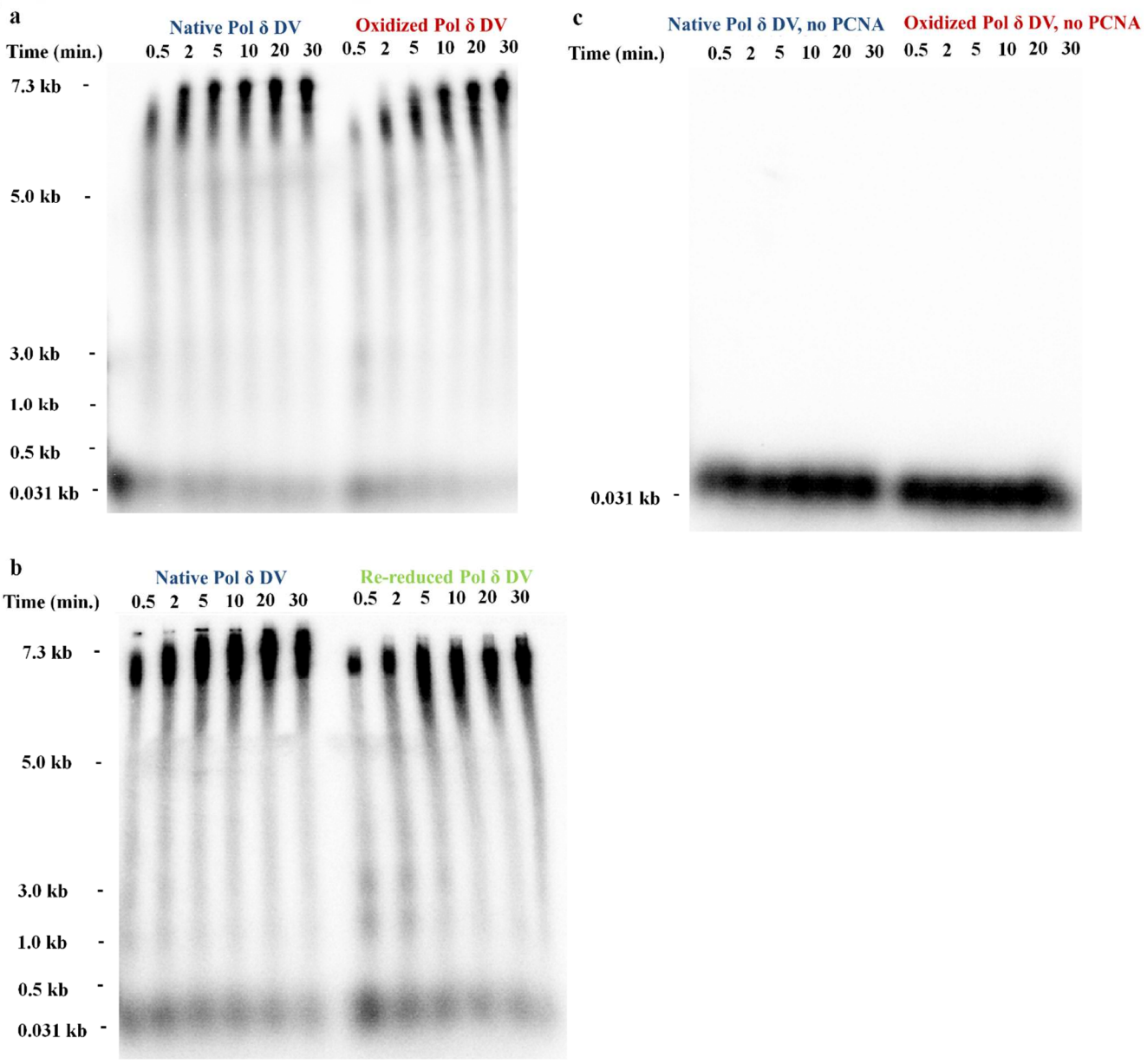

Figure S6. Complete alkaline agarose gels from Figure 2 and control lacking PCNA. The gels include untreated and oxidized Pol δ DV with 5.0 nM PCNA (**a**), untreated and re-reduced Pol δ DV (**b**), and untreated and oxidized Pol δ DV in the absence of PCNA (**c**). No DNA synthesis occurs in the absence of PCNA, confirming that the observed activity in native and oxidized samples is processive.

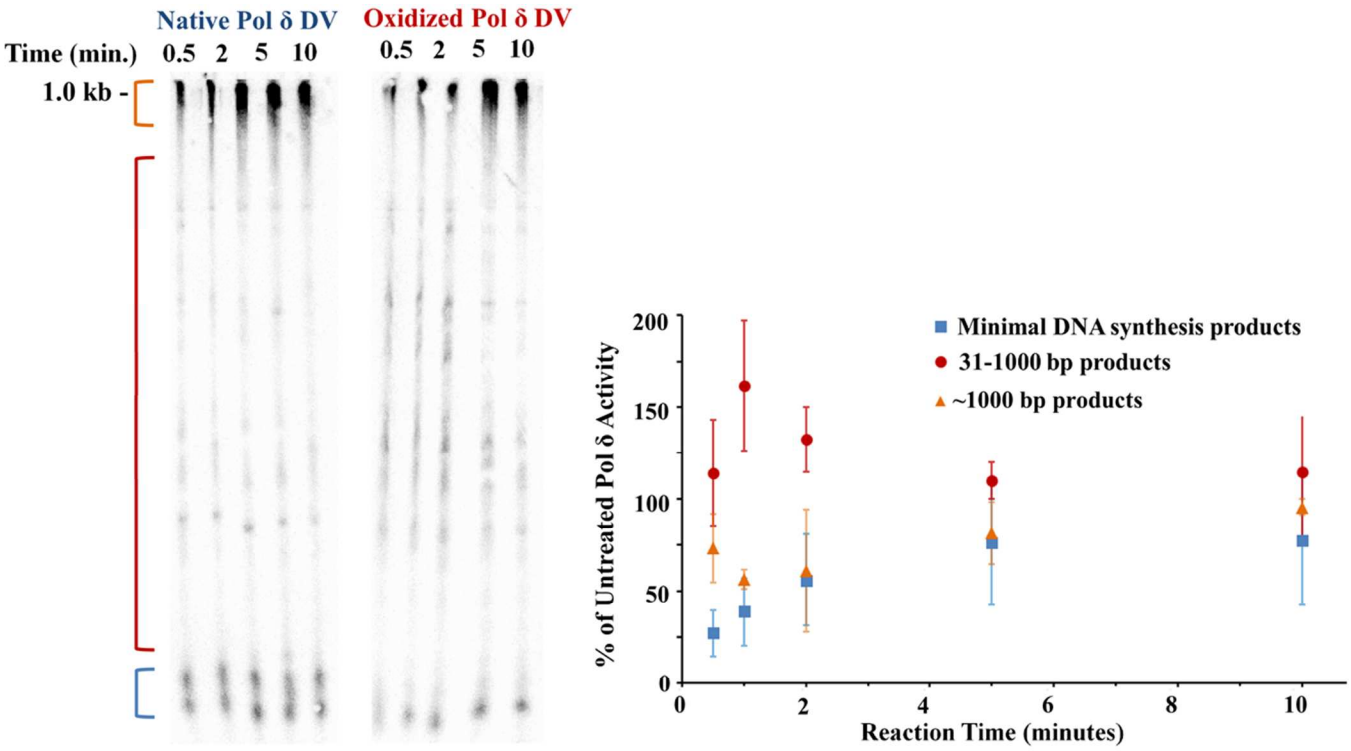

Figure S7. Establishment of activity by oxidized Pol δ. To see if oxidized Pol δ remained active or stalled completely, 0.01% heparin was included in reactions to challenge synthesis and products were analyzed on a 5% denaturing polyacrylamide gel to resolve DNA between 30 and 1000 bp (left). Pol δ remains active after oxidation, primarily forming intermediate-sized products (red range on gel). Native Pol δ is more sensitive to heparin, with more DNA close to primer length (blue range), but when it does associate with DNA, most products are around the maximum size (orange range). These results are consistent with tighter binding and slower processive DNA synthesis by the oxidized form. Gels were quantified using ImageQuant software; as synthesis appears as smears at this resolution, the total amount of background-subtracted radioactivity in each major range shown was compared between untreated and oxidized Pol δ. Error bars are standard deviation of the mean (n = 3).

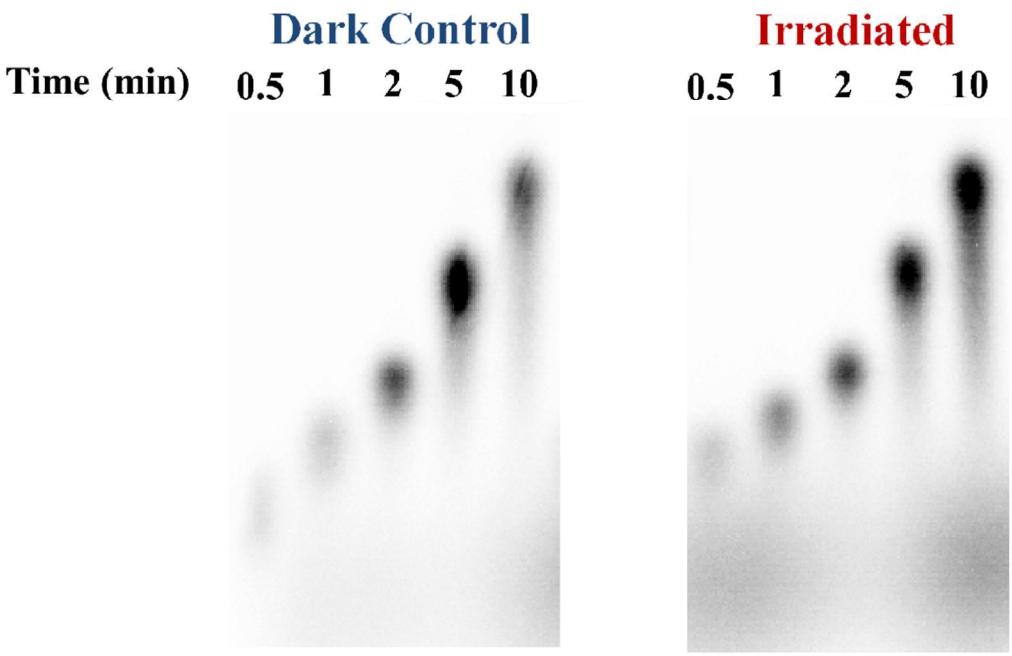

Figure S8. AQ assay controls with 140 nM *E. coli* Klenow fragment exo$^-$. UVA irradiation in the presence of AQ-primed DNA had no significant effect on DNA synthesis by Klenow fragment. The lack of difference confirms that irradiation in the presence of AQ does not adversely affect polymerase enzymes, and further supports the assignment of attenuated activity in Pol δ under the same conditions to [4Fe4S] cluster oxidation.

SI References

(64) Slinker, J. D.; Muren, N. B.; Gorodetsky, A.A.; Barton, J. K. *J. Amer. Chem. Soc.* **2010**, *132*, 2769–2774.

(65) Barton, J.K.; Bartels, P.L.; Deng, Y.; O'Brien, E. *Methods Enzymol.* **2017**, *591*, 355–414.